Joint Sparse Concentric Array Design for Frequency and Rotationally Invariant Beampattern

Yaakov Buchris, *Member, IEEE*, Israel Cohen, *Fellow, IEEE*, Jacob Benesty, and Alon Amar, *Member, IEEE*

***Abstract*—Frequency-invariant concentric arrays are fundamental components in some real-world applications, like teleconferencing, voice service devices, underwater acoustics, and others, where the azimuthal arrival direction of the desired signal is varying. The fact that the demand for limited hardware and computational resources in such applications is essential, motivates the use of a sparse design which can optimize both the number of the required sensors and the complex weights of the beamformer. Herein, we propose a new greedy based joint-sparse design of frequency and rotationally invariant concentric arrays which preserves the properties of the designed directivity pattern for different azimuthal directions of steering. Simulation results show that the greedy sparse design, compared to uniform and random designs, gives superior performance in terms of array gain, and frequency and rotationally invariant beampattern, with a reasonable computational and hardware resources.**

***Index Terms*—Concentric arrays, frequency-invariant beamformer, rotationally-invariant beamformer, greedy joint sparse, superdirective beamformer.**

I. Introduction

MANY real-world applications use sensor arrays and beamforming in order to spatially filter desired signals while suppressing other interfering signals and noise. In the general case, volumetric spherical arrays [1] may be used, as steering can be accomplished from any direction of the 3D sphere. Yet, in some practical applications, planar arrays are preferred [2] due to systemic limitations and the possibility to assume a 2D scenario.

One of the popular geometries of planar arrays is the circular and concentric arrays integrated in video conference systems and some voice service devices, which nowadays have become an essential part of human life [3]–[5]. Such geometries are popular in some practical applications requiring variable steering azimuthal direction of the mainlobe while preserving similar performance in terms of array gain and directivity pattern. In particular, concentric arrays that contain several rings of sensors in different radii and provide similar and steerable beampattern for 360° azimuthal coverage, are advantageous also for broadband beamformers as they enable robust and frequency-invariant (FI) beampatterns over a wide range of frequencies [6]. Among several classical approaches for FI beamformer design which were extensively explored during the last decades [7]–[20], the class of sparse design approaches of FI beamformers is of a great interest, since both the beamformer gains as well as the entire number of sensors and their positions are optimized [21]–[25].

Previous work on sparse concentric array design includes stochastic optimization methods, such as genetic algorithm (GA) [26]–[28], modified particle swarm optimization (MPSO) [29], and biogeography-based optimization (BBO) [30]. These approaches take advantage from the stochastic optimization mechanism which mitigates problems of local minima convergence and have a good numerical stability, yielding sparse concentric arrays with lower sidelobes level (SLL), fewer elements, and nearly rotationally-invariant azimuthal coverage. Chatterjee *et al.* [31] apply a differential evolution (DE) algorithm in order to optimize both the radii and the element spacing of each ring, resulting in an array layout with reduced SLL and a smaller number of elements with respect to a uniform array. In [32] an iterative perturbation algorithm is applied in order to get a sparse planar array with a desired beampattern and directivity. Zhao *et al.* [33] propose a hybrid approach which combines both convex optimization and deterministic one in order to determine the number of concentric rings, the ring radii, and the current ring excitations satisfying the requirements on the directivity pattern. Other deterministic design approaches for sparse concentric arrays can be found in [34]–[36]. The main limitation of all these works is that the design was focused mainly on the narrowband case and/or optimization only of the ring radii, each with sensors arranged uniformly along it.

To the best of the authors' knowledge, in contrast with the narrowband case, broadband sparse designs of FI concentric arrays have almost not been addressed in previous works. In [37]–[39] various design approaches for the synthesis of broadband rotationally symmetric sparse concentric arrays are presented. These approaches optimize the suppression of the peak SLL across the bandwidth of interest, but are not considered as FI arrays. Li *et al.* [40] propose an analytical approach for synthesis of FI directivity pattern of concentric arrays over a certain frequency band. In that approach the ring radii and their weights are determined analytically, matched to a specific frequency satisfying a desired beampattern. Then, for each different frequency some connections are established and used to calculate different sets

Manuscript received September 2, 2019; revised February 5, 2020; accepted March 9, 2020. Date of publication March 20, 2020; date of current version April 20, 2020. This work was supported in part by the Israel Science Foundation under Grant 576/16 and in part by the ISF-NSFC Joint Research Program under Grant 2514/17. The associate editor coordinating the review of this manuscript and approving it for publication was Dr. Andy W. H. Khong. *(Corresponding author: Yaakov Buchris.)*

Yaakov Buchris, Israel Cohen, and Alon Amar are with the Electrical Engineering, Technion Israel Institute of Technology, Haifa 32000, Israel (e-mail: sbucris@gmail.com; icohen@ee.technion.ac.il; aamar@technion.ac.il).

Jacob Benesty is with the Universite du Quebec INRS-EMT, Montreal, QC H5A 1K6, Canada (e-mail: benesty@emt.inrs.ca).

Digital Object Identifier 10.1109/TASLP.2020.2982287

of coefficients that yield the same directivity pattern. The main shortcomings of that approach is that it does not provide enough frequency range coverage over which the beampattern is nearly FI, and it does not optimize the total number of sensors in the array layout.

Motivated by the aforementioned shortcomings of previous approaches, in this paper, we extend our recent work on joint-sparse design of FI beamforming [41], and propose a new greedy based joint-sparse design for FI concentric arrays, which optimizes both the number of sensors and the number of rings while taking into consideration the requirement regarding the rotationally-invariant property. Therefore, the obtained sparse array layout may allow to get a similar array response for different azimuthal directions of steering. Moreover, it also supports the case that one is interested on a similar array response only for an azimuthal sector or for a discrete number of azimuthal directions. The proposed approach is more general with respect to [41] as it allows more than one fixed steering direction. Note that in this work we focus on the two-dimensional (2D) scenario where both the array and the incoming signals are on the same plane. Such a model approximates real scenarios where most of the reflected signals arrive from the walls and less from the floor and the ceiling, e.g., a concentric array in a video conference room. The more general three-dimensional (3D) scenario is out of the scope of this work.

Note that since it is desired to determine an array layout which supports optimal steering from more than one possible direction, the optimization problem cannot be solved directly, as multiple distortionless constraints should be imposed simultaneously, leading to a contradiction. Instead, we derive a four-step sparse design where we split our problem into a subproblem of determining the array layout for steering from a certain direction, then we multiply the obtained array layout for additional directions corresponding to other desired steering directions, followed by a redundancy removal step where a final sparse array layout is obtained and used for synthesis.

As a first step of the proposed design, a modified orthogonal matching pursuit (OMP) [42], [43] greedy based iterative algorithm is applied aiming to determine the array layout for a case of steering to a fixed direction. In each iteration, it seeks for the sensors that mostly contribute to the residual signal. As a stopping criterion, the selected set of sensors up to the current iteration, which are joint to all the frequency bins in the bandwidth of interest, are used to construct the array layout steered to the fixed direction while fulfilling several desired constraints. In the next step, the array layout is symmetrically duplicated into additional azimuthal directions in order to obtain nearly rotationally-invariant beampattern. As the duplicated array layout contains some redundancy, an ℓ_{12}-optimization problem is solved in order to attain a more compact array layout which is joint sparse both in the number of rings and in the number of sensors, used in the final synthesis step to obtain the rotationally-invariant FI beampattern. Reducing also the number of rings may contribute to the rotationally-invariant property of the sparse array. The fact that the array layout is joint-sparse implies on the desired property of hardware consuming since the selected sensors are joint for all the frequencies in the bandwidth of interest.

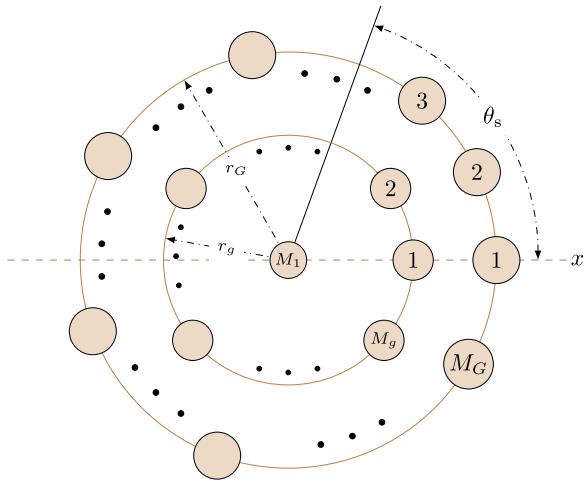

Fig. 1. Illustration of a concentric circular array with G rings, where the gth ($g = 1, 2, \ldots, G$) ring, with a radius of r_g, consists of M_g omnidirectional microphones, with θ_s being the source incidence angle.

Simulation results compare between the proposed greedy sparse design, a uniform array design and a random array design. It is shown that the greedy sparse design yields a FI rotationally-invariant beamformer with a better white noise gain (WNG) and high directivity. In contrast, the uniform designs suffer from high SLL and sensitivity to noise, while the random design provides unstable and fluctuating results. In addition, the sparse design requires reasonable resource consumption leading to a practical design for applications involving large arrays with hundreds of candidate sensors.

II. Signal Model and Problem Formulation

Assume a 2D scenario during which signals are propagating towards a concentric array composed of G rings, where the gth ring is characterized by its radius, $r_g,\ g = 1, 2, \ldots, G$, and the number of candidate positions for locating the sensors, M_g, as illustrated in Fig. 1. The total number of candidate positions is $M = \sum_{g=1}^{G} M_g$. The center of the concentric array coincides with the first ring having $r_1 = 0$ and M_1=1. The direction of arrival of signals towards the array is denoted by the azimuth θ, measured anti-clockwise from the x axis, i.e., at $\theta = 0^\circ$, and sensor 1 of each ring is placed on the x axis, i.e., at $\theta = 0^\circ$. The direction of arrival of the desired source signal to the array is denoted by the azimuth angle θ_s.

Let Ω and Θ denote the frequency and angle ranges of interest, respectively. We uniformly discretize both the frequency and angle spaces and introduce J frequency bins $\{\omega_j\}_{j=1}^{J} \in \Omega$, and P directions $\{\theta_p\}_{p=1}^{P} \in \Theta$ that cover the entire beampattern, i.e., $\Theta \in [-\pi, \pi]$.

The beampattern of such an array for the angular frequency $\omega_j \in \Omega$ and azimuth $\theta_p \in \Theta$ can be expressed as

$$\mathcal{B}(\omega_j, \theta_p) = \mathrm{Trace}\left[\mathbf{H}^H(\omega_j)\mathbf{D}(\omega_j, \theta_p)\right], \quad (1)$$

where the superscript ^{H} denotes the conjugate-transpose operator, the matrix

$$\mathbf{H}(\omega) = \begin{bmatrix} H_{1,1}(\omega_j) & \cdots & H_{1,g}(\omega_j) & \cdots & H_{1,G}(\omega_j) \\ 0 & \cdots & H_{2,g}(\omega_j) & \cdots & H_{2,G}(\omega_j) \\ \vdots & \cdots & H_{3,g}(\omega_j) & \cdots & H_{3,G}(\omega_j) \\ 0 & \cdots & \vdots & \cdots & H_{4,G}(\omega_j) \\ 0 & \cdots & H_{M_g,g}(\omega_j) & \cdots & \vdots \\ 0 & \cdots & 0 & \cdots & H_{M_G,G}(\omega_j) \end{bmatrix} \tag{2}$$

is an $M_G \times G$ matrix, whose gth column contains the beamformer coefficients located on the gth ring, while we assume that $1 = M_1 \leq M_2 \leq \ldots, \leq M_G$. The matrix $\mathbf{D}(\omega_j, \theta_p)$ is an $M_G \times G$ steering matrix whose gth column is given by [2]

$$\mathbf{d}_g(\omega_j, \theta_p) = \begin{bmatrix} e^{\jmath \frac{\omega_j r_g}{c} \cos(\theta_p - \psi_{g,1})} \\ e^{\jmath \frac{\omega_j r_g}{c} \cos(\theta_p - \psi_{g,2})} \\ \vdots \\ e^{\jmath \frac{\omega_j r_g}{c} \cos(\theta_p - \psi_{g,M_g})} \\ 0 \\ 0 \end{bmatrix}, \tag{3}$$

where

$$\psi_{g,m} = \frac{2\pi(m-1)}{M_g},\ m = 1, 2, \ldots, M_g \tag{4}$$

is the angular position of the mth array element of the gth ring, $\jmath = \sqrt{-1}$, and c is the waveform's speed.

Assume that we select a subset of $K \ll M$ sensors, concentrated in $G' < G$ rings, used to synthesize the K spatio-temporal beampatterns for each frequency $\omega_j \in \Omega$, that is,

$$\mathcal{B}_K(\omega_j, \theta_p) = \mathcal{Q}\{\mathbf{H}(\omega_j); \mathbf{A}_K(\mathbf{i}_{G'})\}^H \mathcal{Q}\{\mathbf{D}(\omega_j, \theta_p); \mathbf{A}_K(\mathbf{i}_{G'})\}, \tag{5}$$

where $\mathcal{Q}\{\cdot\}$ is a FI selection operator defined as follows: for matrices $\mathbf{X}_1$ and $\mathbf{X}_2$ of size $m \times n$, $\mathcal{Q}\{\mathbf{X}_1; \mathbf{X}_2\}$ returns a column vector with all the entries in $\mathbf{X}_1$ for which the corresponding entries in the binary matrix $\mathbf{X}_2$ are equal to '1'. The matrix $\mathbf{A}_K(\mathbf{i}_{G'})$ of size $M_G \times G$ contains K nonzero elements which spread across only G' columns, whose indices are specified by the $G' \times 1$ vector $\mathbf{i}_{G'}$. Note that for the particular case that $\mathcal{Q}\{\cdot\}$ operates on vectors $\mathbf{x}_1$ and $\mathbf{x}_2$ of size n, where the binary vector $\mathbf{x}_2$ contains $n' \leq n$ nonzero elements, we simply get that

$$\mathcal{Q}\{\mathbf{x}_1; \mathbf{x}_2\} = \mathbf{T}_{\mathrm{s}}(\mathbf{i}_{n'}(\mathbf{x}_2))\, \mathbf{x}_1, \tag{6}$$

where the vector $\mathbf{i}_{n'}(\mathbf{x}_2)$ of length n' contains the indices of the nonzero entries of the vector $\mathbf{x}_2$, and $\mathbf{T}_{\mathrm{s}}(\mathbf{i}_{n'}(\mathbf{x}_2))$ is an $n' \times n$ FI selection matrix, i.e., containing n' rows of an $n \times n$ identity matrix corresponding to the nonzero indices of the vector $\mathbf{x}_2$. Note that the following property is satisfied: $\mathbf{T}_{\mathrm{s}}(\mathbf{i}_n) = \mathbf{I}_n$ where $\mathbf{i}_n = [1, 2, \ldots, n]^T$ and $\mathbf{I}_n$ is the $n \times n$ identity matrix.

Let the function $\mathcal{B}_{\mathrm{d}}^{\theta_{\mathrm{s}}}(\theta), \theta, \theta_{\mathrm{s}} \in \Theta$, be a desired far-field FI beampattern in the bandwidth of interest Ω, with a mainlobe steered to θ_{s}. Our goal is stated as follows: we want that the synthesized beampattern $\mathcal{B}_K(\omega_j, \theta_p), \forall \omega_j \in \Omega$, with the structure specified by (5), will be FI but at the same time will be as close as possible to the desired power beampattern, $\mathcal{B}_{\mathrm{d}}^{\theta_{\mathrm{s}}}(\theta)$ (in the mean-squared error sense), under some design constraints to be specified below. Additionally, the K selected sensors should also support the rotationally-invariant property of circular arrays in general, and of concentric arrays in particular, meaning that approximately similar response can be obtained for different values of the steering direction, θ_{s}. For example, assume that the K selected sensors are used to synthesize the beampattern $\mathcal{B}_K^{(1)}(\omega_j, \theta_p), \forall \omega_j \in \Omega, \forall \theta_p \in \Theta$ being similar to $\mathcal{B}_{\mathrm{d}}^{\theta_{\mathrm{s}}}(\theta)$ with the following overall error:

$$\sum_{j=1}^{J} \sum_{p=1}^{P} |\mathcal{B}_{\mathrm{d}}^{\theta_{\mathrm{s}}}(\theta_p) - \mathcal{B}_K^{(1)}(\omega_j, \theta_p)|^2 \leq \epsilon_{\mathrm{t}}^2, \tag{7}$$

where ϵ_{t} is a small positive parameter, then the same K sensors can be used to synthesize also $\mathcal{B}_K^{(2)}(\omega_j, \theta_p), \forall \omega_j \in \Omega, \forall \theta_p \in \Theta$ being similar to $\mathcal{B}_{\mathrm{d}}^{\tilde{\theta}_{\mathrm{s}}}(\theta)$ with similar accuracy (i.e., similar ϵ_{t}^2), while $\tilde{\theta}_{\mathrm{s}} = \theta_{\mathrm{s}} + \Delta\theta_{\mathrm{s}}$ and $\mathcal{B}_{\mathrm{d}}^{\tilde{\theta}_{\mathrm{s}}}(\theta)$ is a shifted version of $\mathcal{B}_{\mathrm{d}}^{\theta_{\mathrm{s}}}(\theta)$ by $\Delta\theta_{\mathrm{s}}$ degrees.

The structure of the synthesized beampattern $\mathcal{B}_K(\omega_j, \theta_p)$ with the K sensors concentrated in $G' < G$ rings may contribute to obtain the rotationally-invariant property by minimizing G'. The intuition for this constraint is as follows: consider the case that the array layout obtained by the K sensors is linear and a second case where all the sensors are concentrated in a single ring. In the first case where all the rings are used, the linear geometry can provide sparse robust design as presented in [41], yet it clearly does not support the rotationally-invariant property. In the second case, we get nearly rotationally-invariant circular array but may obtain limited performance in terms of robust FI beampattern. The intermediate cases with a small number of rings used to construct the array layout are expected to yield a compromise between robustness and rotationally invariance. In light of this trade-off, we impose that the K selected sensors will be concentrated on $G' < G$ rings.

III. Typical Design Constraints

Herein, we present several constraints that should be taken into consideration while designing concentric FI beamformers. Denote the vector $\mathbf{h}(\omega_j)$ of length M containing the nonzero elements of the matrix $\mathbf{H}(\omega_j)$ arranged in a column vector of length M, that is,

$$\mathbf{h}(\omega_j) = [H_{1,1}(\omega_j))\ H_{2,1}(\omega_j) \cdots H_{2,M_2}(\omega_j) \cdots\ H_{G,1}(\omega_j) \cdots H_{G,M_G}(\omega_j)]^T, \tag{8}$$

where the superscript ^{T} denotes the transpose operator, and the mth element corresponds to the mth candidate sensor whose

position is denoted by $\mathbf{p}_m,\ m = 1, 2, \ldots, M$, given as [44]

$$\{\mathbf{p}_m\}_{m=1}^{M} \in \left\{ \begin{bmatrix} r_g \cos(\psi_{g,m_g}) \\ r_g \sin(\psi_{g,m_g}) \end{bmatrix} \right\}, \quad m_g = 1, \ldots, M_g, g = 1, \ldots, G. \tag{9}$$

Similarly, define also the vector $\mathbf{d}(\omega_j, \theta_p)$ of length M containing the nonzero elements of the matrix $\mathbf{D}(\omega_j, \theta_p)$ arranged in a column vector. We set $P' < P$ directions that cover the mainlobe region Θ_{m}, where the subscript m stands for mainlobe, and the remaining $P - P'$ directions that cover the sidelobe region Θ_{s} where the subscript s stands for sidelobe.

The first constraint is a mainlobe constraint formulated as multiple joint-sparse constraints, that is, $\forall \omega_j \in \Omega$, [41]

$$\mathcal{C}_1 : \left\| (b_{\mathrm{d}}^{\mathrm{m}}(\theta_{\mathrm{s}}))^T \mathbf{h}^H(\omega_j) \mathbf{T}_{\mathrm{s}}^T(\mathbf{i}_K) \mathbf{T}_{\mathrm{s}}(\mathbf{i}_K) \mathbf{D}_{M,\Theta_{\mathrm{m}}}(\omega_j) \right\|_2^2 \leq \epsilon_1(\omega_j), \tag{10}$$

where $\mathbf{i}_K = [i_1, i_2, \ldots, i_K]^T$ is a vector containing the indices of the K chosen sensors located at $\{\mathbf{p}_{i_k}\}_{k=1}^{K}$, $\epsilon_1(\omega_j)$ is a small positive parameter, $||\cdot||_2$ is the ℓ_2-norm,

$$\mathbf{D}_{M,\Theta_{\mathrm{m}}}(\omega_j) = [\mathbf{d}(\omega_j, \theta_1), \mathbf{d}(\omega_j, \theta_2), \ldots, \mathbf{d}(\omega_j, \theta_{P'})] \tag{11}$$

is an $M \times P'$ matrix, and

$$b_{\mathrm{d}}^{\mathrm{m}}(\theta_{\mathrm{s}}) = \left[\mathcal{B}_{\mathrm{d}}^{\theta_{\mathrm{s}}}(\theta_1), \mathcal{B}_{\mathrm{d}}^{\theta_{\mathrm{s}}}(\theta_2), \ldots, \mathcal{B}_{\mathrm{d}}^{\theta_{\mathrm{s}}}(\theta_{P'}) \right]^T \tag{12}$$

is a vector containing samples of the desired beampattern in the directions covering the mainlobe.

Similarly, for the sidelobe constraint we can obtain multiple joint-sparse constraints, and write $\forall \omega_j \in \Omega$,

$$\mathcal{C}_2 : \left\| (b_{\mathrm{d}}^{\mathrm{s}}(\theta_{\mathrm{s}}))^T - \mathbf{h}^H(\omega_j) \mathbf{T}_{\mathrm{s}}^T(\mathbf{i}_K) \mathbf{T}_{\mathrm{s}}(\mathbf{i}_K) \mathbf{D}_{M,\Theta_{\mathrm{s}}}(\omega_j) \right\|_2^2 \leq \epsilon_2(\omega_j), \tag{13}$$

where $\epsilon_2(\omega_j)$ is a small positive parameter. The matrix $\mathbf{D}_{M,\Theta_{\mathrm{s}}}(\omega_j)$ is defined similarly to $\mathbf{D}_{M,\Theta_{\mathrm{m}}}(\omega_j)$, and the vector $b_{\mathrm{d}}^{\mathrm{s}}(\theta_{\mathrm{s}})$ is defined similarly to $b_{\mathrm{d}}^{\mathrm{m}}(\theta_{\mathrm{s}})$.

Clearly, imposing only $\mathcal{C}_1$ and $\mathcal{C}_2$ does not ensure that the array responses $\mathcal{B}_K(\omega_j, \theta_p),\ \omega_j \in \Omega$ will not distort the signal of interest and especially that they will be robust to array calibration and model mismatch errors. Hence, we include additional constraints. The first is the well known distortionless response constraint, stating that, $\forall \omega_j \in \Omega$,

$$\mathcal{C}_3 :\ \mathbf{h}^H(\omega_j) \mathbf{T}_{\mathrm{s}}^T(\mathbf{i}_K) \mathbf{T}_{\mathrm{s}}(\mathbf{i}_K) \mathbf{d}(\omega_j, \theta_{\mathrm{s}}) = 1, \tag{14}$$

and the second is the limitation of the white noise output power, given as, $\forall \omega_j \in \Omega$,

$$\mathcal{C}_4 :\ \mathbf{h}^H(\omega_j) \mathbf{T}_{\mathrm{s}}^T(\mathbf{i}_K) \mathbf{T}_{\mathrm{s}}(\mathbf{i}_K) \mathbf{h}(\omega_j) \leq \gamma(\omega_j), \tag{15}$$

where $\gamma(\omega_j)$ is a parameter expressing the maximal allowed white noise output power at frequency ω_j. Note that due to the distortionless constraint specified by (14), the formulation of (15) is equivalent to restricting the WNG of the array to be above a certain threshold value [2, ch.6]. The WNG for the general case of a beamformer coefficient vector $\mathbf{h}(\omega_j)$ [44],

$$\mathcal{W}(\mathbf{h}(\omega_j)) = \frac{\left| \mathbf{h}^H(\omega_j) \mathbf{d}(\omega_j, \theta_{\mathrm{s}}) \right|^2}{\mathbf{h}^H(\omega_j) \mathbf{h}(\omega_j)}, \tag{16}$$

is a measure indicating the array gain in the presence of uncorrelated white noise. It also indicates the sensitivity of the array to model mismatch errors [2].

In the framework of sparse design of concentric arrays we may define two additional constraints. The first is a symmetry of the designed beampattern with respect to the steering direction, θ_{s}. The motivation to such constraint is as explained above that we would like the final array layout to include as few rings as possible, thus, it may lead to a better rotationally-invariant response.

Assuming that $\theta_{\mathrm{s}} = 0^\circ$, we may arrange all the candidate sensors in symmetric pairs, while sensors that lay on the main axis (i.e., the x axis presented in Fig. 1) are symmetric to themselves, that is, we have $M' \leq M$ symmetric pairs. Without loss of generality, we assume that $M'' \leq M'$ are pairs of sensors that do not lay on the main axis, while the remaining $M' - M''$ sensors correspond to the sensors on the main axis.

Let the matrix $\mathbf{S}$ be a matrix of size $M' \times M$ where each of its first M'' rows contain zeros except two entries of '1's corresponding to the indices of the mth symmetric pair ($m = 1, 2, \ldots, M''$). The entries of the remaining $M' - M''$ sensors laying on the main axis, are equal to '2'. As a simple example to illustrate the structure of the matrix $\mathbf{S}$, we consider a concentric array with two rings, the inner ring has four sensors locating in the azimuthal directions $\psi_{1,1} = 0^\circ, \psi_{1,2} = 90^\circ, \psi_{1,3} = 180^\circ$, and $\psi_{1,4} = 270^\circ$. The external ring has five sensors locating at the azimuthal directions $\psi_{2,1} = 0^\circ, \psi_{2,2} = 72^\circ, \psi_{2,3} = 144^\circ, \psi_{2,4} = 216^\circ$ and $\psi_{2,5} = 288^\circ$. Therefore, three sensors out of the nine sensors lay on the main axis, while three more pairs do not lay on the main axis. Consequently, the corresponding matrix is

$$\mathbf{S} = \begin{bmatrix} 0 & 1 & 0 & 1 & 0 & 0 & 0 & 0 & 0 \\ 0 & 0 & 0 & 0 & 0 & 1 & 0 & 0 & 1 \\ 0 & 0 & 0 & 0 & 0 & 0 & 1 & 1 & 0 \\ 2 & 0 & 0 & 0 & 0 & 0 & 0 & 0 & 0 \\ 0 & 0 & 2 & 0 & 0 & 0 & 0 & 0 & 0 \\ 0 & 0 & 0 & 0 & 2 & 0 & 0 & 0 & 0 \end{bmatrix}. \tag{17}$$

The symmetry constraint is formulated as, $\forall \omega_j \in \Omega$,

$$\mathcal{C}_5 : \left\| \tilde{\mathbf{S}} \mathbf{h}(\omega_j) \right\|_2^2 \leq \epsilon_3(\omega_j), \tag{18}$$

where $\epsilon_3(\omega_j)$ is a small positive parameter, and $\tilde{\mathbf{S}}$ contains the first M'' rows of the matrix $\mathbf{S}$. Note that we take only the rows of pairs that do not lay on the main axis. We later use all the rows of the matrix $\mathbf{S}$.

The second additional constraint relates to the desired property of rotationally-invariant beampattern. As discussed before we would like to get a similar response for different values of the steering direction, θ_{s}. Thus, we may formulate the following

rotationally-invariant constraint as, $\forall\theta_{\rm s}\in\Theta$,

$$\mathcal{C}_6:\sum_{j=1}^{J}\sum_{p=1}^{P}|\mathcal{B}_{\rm d}^{\theta_{\rm s}}(\theta_p)-\mathcal{B}_K(\omega_j,\theta_p)|^2\le\epsilon_{\rm t}^2. \tag{19}$$

Combining constraints $\mathcal{C}_1,\mathcal{C}_2,\mathcal{C}_3,\mathcal{C}_4,\mathcal{C}_5,\mathcal{C}_6$, we can formulate the general joint-sparse rotationally-invariant problem of interest as

$$\begin{aligned}&\text{minimize }\{K,G'\}\\&\text{subject to }\ \mathcal{C}_1,\mathcal{C}_2,\mathcal{C}_3,\mathcal{C}_4,\mathcal{C}_5,\mathcal{C}_6,\ \forall\omega_j\in\Omega,\end{aligned} \tag{20}$$

whose solution yields the jointly-sparse filters:

$$\mathbf{h}_K(\omega_j)=\mathbf{T}_{\rm s}(\mathbf{i}_K)\,\mathbf{h}(\omega_j),\ \forall\omega_j\in\Omega. \tag{21}$$

In this work, we solve (20) by extending our recent incoherent sparse FI design [41], and propose a greedy-based sparse approach to design of concentric arrays. Based on a joint sparse version of the OMP algorithm [45]–[47], $K'\le K$ joint-sparse sensors are selected, which comply constraints $\mathcal{C}_1$–$\mathcal{C}_5$. In order to comply $\mathcal{C}_6$, the obtained array layout is duplicated and an additional ℓ_{12} optimization is performed aiming to obtain an array layout which is sparse both in the number of sensors and in the number of rings. The proposed approach has much lower computational burden, which makes it more feasible for practical designs, especially when the number of candidate sensors is an order of hundreds or more. Additionally, in a future research on this topic, we may consider designs of 3D sparse arrays. Due to the greedy algorithm, such an extension may lead also to a moderate increase of the affordable computational complexity.

IV. A Greedy Based Design of FI Sparse Concentric Arrays

In this section, we present a four-step greedy based approach for solving (20) and obtain a sparse design of an FI concentric beamformer. Note that while in our previous incoherent design the task of determining the parameter K was not trivial, in the proposed greedy design it may be much more intuitive and straightforward. In the following subsections, we describe each of these steps.

A. Determining the Array Layout for Steering From Endfire

The first step includes a greedy search of the best $K'\le K$ sensors over all the candidate sensors that fulfill the above constraints. We may assume that the desired signal arrives from the endfire direction (i.e. $\theta_{\rm s}=0^\circ$), while other interfering signals arrive from different arbitrary directions. As we are looking for an FI beampattern, the problem would be formulated as a joint-sparse greedy search one. One of the popular tools for implementing greedy-based search algorithms is the OMP. Applying the OMP directly to our problem is not a trivial task, since it is desired to obtain a sparse array layout which is joint to all the frequencies in the bandwidth of interest. Thus, in the following we derive a modified version of OMP.

Let us consider the matrix $\mathbf{D}_j$, of size $P\times M$, to be the concatenation of the matrices $\mathbf{D}_{M,\Theta_{\rm m}}^H(\omega_j)$ and $\mathbf{D}_{M,\Theta_{\rm s}}^H(\omega_j)$, i.e.,

$$\mathbf{D}_j=\begin{bmatrix}\mathbf{D}_{M,\Theta_{\rm m}}^H(\omega_j)\\ \mathbf{D}_{M,\Theta_{\rm s}}^H(\omega_j)\end{bmatrix}. \tag{22}$$

We treat the matrix $\mathbf{D}_j$ as a dictionary containing in each column one word of length P, also called an atom, which corresponds to one of the M candidate sensors. It is desired to express $\mathcal{B}_{\rm d}^{\theta_{\rm s}}(\theta)$ with atoms from the dictionary by finding a vector $\mathbf{h}^{\rm uc}(\omega_j)\in\mathbb{C}^M$ which solves the following problem:

$$\mathbf{D}_j\mathbf{h}^{\rm uc}(\omega_j)=\mathbf{b}_{\rm d}(\theta_{\rm s}), \tag{23}$$

where

$$\mathbf{b}_{\rm d}(\theta_{\rm s})=\begin{bmatrix}\mathbf{b}_{\rm d}^{\rm m}(\theta_{\rm s})\\ \mathbf{b}_{\rm d}^{\rm s}(\theta_{\rm s})\end{bmatrix} \tag{24}$$

is the desired beampattern, and the superscript uc stands for unconstrained.

Since typically $\mathbf{D}_j$ is an under-determined matrix, i.e., the linear system of equations that it represents is under-determined, (23) has infinite solutions. Among them, the class of sparse solutions with few nonzero elements is of a great interest because it means that practically small number of sensors is required to construct the desired beampattern.

Mathematically, the solution with the fewest nonzero elements can be found by solving the NP-hard ℓ_0-norm problem:

$$\min\|\mathbf{h}^{\rm uc}(\omega_j)\|_0\ \text{ subject to }\mathbf{D}_j\mathbf{h}^{\rm uc}(\omega_j)=\mathbf{b}_{\rm d}(\theta_{\rm s}), \tag{25}$$

where $\|\mathbf{x}\|_0$ is the number of nonzero elements in the vector $\mathbf{x}$. One way to solve (25) is by modifying it to the ℓ_1-norm optimization problem [48]:

$$\min\|\mathbf{h}^{\rm uc}(\omega_j)\|_1\ \text{ subject to }\mathbf{D}_j\mathbf{h}^{\rm uc}(\omega_j)=\mathbf{b}_{\rm d}(\theta_{\rm s}). \tag{26}$$

Instead of solving (25) by an ℓ_1 optimization like in [41], it can be solved using the OMP algorithm which finds $\mathbf{h}^{\rm uc}(\omega_j)$ element by element in the step-by-step iterative greedy manner. In other words, we would like to find greedily an approximation to the P length vector $\mathbf{b}_{\rm d}(\theta_{\rm s})$ using as small as possible number of atoms from the dictionary matrix, $\mathbf{D}_j$. In order to solve (25) using OMP, it is useful to consider the mutual coherence of the matrix, $\mathbf{D}_j$, defined as [49]

$$\mu(\mathbf{D}_j)=\max_{k\ne l}\frac{|\mathbf{d}_{j_l}^H\mathbf{d}_{j_k}|}{\|\mathbf{d}_{j_l}\|_2\|\mathbf{d}_{j_k}\|_2}, \tag{27}$$

where $\mathbf{d}_{j_l}$ is the lth column of the matrix $\mathbf{D}_j$. The following theorem indicates whether a sparse signal can be recovered uniquely by the OMP algorithm.

Theorem: Let $\mathbf{x}\in\mathbb{C}^n$ being a k-sparse vector, meaning that it has up to k nonzero elements. For the model $\mathbf{A}\mathbf{x}=\mathbf{b}$, where $\mathbf{b}\in\mathbb{C}^m$, $\mathbf{A}\in\mathbb{C}^{m\times n}$, $n\gg m$ are given, $\mathbf{x}$ can be recovered uniquely by the OMP algorithm if $\mathbf{A}$ and $\mathbf{x}$ satisfy [50]

$$\mu(\mathbf{A})<\frac{1}{2k-1}. \tag{28}$$

Equivalently, if

$$k < \frac{1}{2}\left(\frac{1}{\mu(\mathbf{A})}+1\right), \tag{29}$$

then $\mathbf{x}$ can be recovered uniquely from a given $\mathbf{A}$ and $\mathbf{b}$ using the OMP algorithm.

In the Appendix we derive the mutual coherence of the matrix $\mathbf{D}_j$ to be

$$\mu(\mathbf{D}_j) = \max_{k\neq l}\left| I_0\left(\sqrt{-\frac{\omega_j^2}{c^2}\left[r^2(\mathbf{p}_l)+r^2(\mathbf{p}_k)-\mathbf{p}_l^T\mathbf{p}_k\right]}\right)\right|, \tag{30}$$

where $r(\mathbf{p}_m)$ denotes the radius the mth sensor located at $\mathbf{p}_m$, and $I_0(\cdot)$ is the modified Bessel function of the first kind. Substituting typical values to the parameters that appear in (30) like those presented later in Section V, one may see that (29) does not hold for $k>0$, meaning that the matrix $\mathbf{D}_j$ does not satisfy the above theorem. This can be explained since in our setup the desired beampattern is indeed not a pure sparse vector but an approximated one, which has a non-unique sparse representation. Therefore, our dictionary has high mutual coherence implying that it has some redundancy which will be exploited to obtain higher performance. In the following we may obtain an approximated sparse version of the beampattern. In the literature, very few previous works considered sparse algorithms with coherent and redundant dictionaries [51], [52]. Yet, they consider the simple narrowband sparse case rather than the joint-sparse one. In order to mitigate the influence of the high mutual coherence, herein, we employ a mask in order to reduce the possibility to chose different atoms with high similarity.

The joint-sparse OMP algorithm contains the following steps.

1) Initialization: Initialize, $\forall\omega_j\in\Omega$, the vectors:

$$\mathbf{r}^{(0)}(\omega_j) = \mathbf{b}_{\mathrm{d}}(\theta_{\mathrm{s}}) \tag{31}$$

of length P to be a residual vector which supposed to approach iteratively to a zero vector, and initialize the sparse vector

$$\mathbf{b}_{\mathrm{g}}^{(0)}(\omega_j) = \mathbf{0}_P, \tag{32}$$

which stores the desired beampattern after the iterative algorithm converges, where $\mathbf{0}_P$ is a zeros vector of length P. We also initialize the vector $\mathbf{i}_{K'}^{(0)}$ which stores the indices of the selected sensors in each iteration.

2) Iterative Greedy Algorithm: Initialize the $M'\times M'$ diagonal weighting matrix $\mathbf{W}^{(0)}=\mathbf{I}_{M'}$, used to assign a low weighting to sensors already chosen in previous iteration and to their neighbors by multiplying the corresponding indices by a mask vector, $\mathbf{m}$, of length $L_{\mathbf{m}}$.

In each iteration of a standard OMP algorithm, it is desired to find the next atom which has the most contribution in the reconstruction of the desired vectors, $\mathbf{b}_{\mathrm{g}}^{(l)}(\omega_j),\ \omega_j\in\Omega$. It is done by projecting the residual signals, $\mathbf{r}^{(l)}(\omega_j),\ \omega_j\in\Omega$, over all the remaining atoms in the current iteration. For the narrowband case the atom with the most contribution maximizes the following term:

$$m_l^{\mathrm{NB}} = \underset{m=1,2,\ldots,M}{\operatorname{argmax}}\left[\left|\mathbf{D}_j^H\mathbf{r}^{(l)}(\omega_j)\right|\right]_m, \tag{33}$$

where $[\mathbf{x}]_i$ denotes the ith element of the vector $\mathbf{x}$, and the superscript NB stands for narrowband. As we are interested to obtain a sparse array layout which is joint $\forall\omega_j\in\Omega$, we have to take it into consideration when we are searching for the sensors that have the largest contribution in the lth iteration. One way to do so, is to sum the contributions over all the frequencies, i.e., to solve the following joint sparse problem [45]–[47], [53]:

$$m_l^{\mathrm{BB}} = \underset{m=1,2,\ldots,M}{\operatorname{argmax}}\left[\sum_{j=1}^{J}\left|\mathbf{D}_j^H\mathbf{r}^{(l)}(\omega_j)\right|\right]_m, \tag{34}$$

where the superscript BB stands for broadband. The dimension of the inner product in the last equations is a vector of length M, where each entry contains a positive value which express the contribution of the corresponding sensor to the residual signal. As discussed before, it is desired to obtain a symmetric solution with respect to the endfire direction, therefore, for the lth iteration we may find the symmetric pair of sensors out of M' that maximizes the function:

$$m_l^{\mathrm{JSBB}} = \underset{m=1,2,\ldots,M'}{\operatorname{argmax}}\left[\mathbf{W}^{(l-1)}\mathbf{S}\sum_{j=1}^{J}\left|\mathbf{D}_j^H\mathbf{r}^{(l)}(\omega_j)\right|\right]_m, \tag{35}$$

where the superscript JSBB stands for joint symmetric broad band, and the matrix $\mathbf{S}$ of size $M'\times M$, is defined similarly like in (17). The meaning of (35) is that we find the pair of symmetric sensors with the largest projection over the desired beampattern across the entire bandwidth.

3) Update: Update the following $L^{(l)}\times 1$ vector:

$$\mathbf{i}_{K'}^{(l)} = \left[\left(\mathbf{i}_{K'}^{(l-1)}\right)^T \quad \left(\mathbf{i}(m_l^{\mathrm{JSBB}})\right)^T\right]^T, \tag{36}$$

where $\mathbf{i}(m_l^{\mathrm{JSBB}})$ contains the indexes of the sensors whose entries are not equal to zero in the corresponding rows of the matrix $\mathbf{S}$.

Let $\mathbf{D}_j(\mathbf{i}_{K'}^{(l)})$ be a matrix of size $L^{(l)}\times P$ containing only the rows of $\mathbf{D}_j$ whose indices are specified by $\mathbf{i}_{K'}^{(l)}$, i.e.,

$$\mathbf{D}_j(\mathbf{i}_{K'}^{(l)}) = \mathbf{T}_{\mathrm{s}}\left(\mathbf{i}_{K'}^{(l)}\right)\mathbf{D}_j, \tag{37}$$

where $\mathbf{T}_{\mathrm{s}}(\mathbf{i}_{K'}^{(l)})$ is an $L^{(l)}\times M$ selection matrix.

We can calculate, $\forall\omega_j\in\Omega$, the projection vector of size $L^{(l)}\times 1$ of the desired beampattern over the chosen atoms up to the lth iteration as

$$\mathbf{h}_{L^{(l)}}^{\mathrm{uc}}(\omega_j) = \left[\mathbf{D}_j^H(\mathbf{i}_{K'}^{(l)})\mathbf{D}_j(\mathbf{i}_{K'}^{(l)})\right]^{-1}\mathbf{D}_j^H(\mathbf{i}_{K'}^{(l)})\mathbf{b}_{\mathrm{d}}(\theta_{\mathrm{s}}), \tag{38}$$

which is used to update the following vectors $\forall\omega_j\in\Omega$:

$$\mathbf{b}_{\mathrm{g}}^{(l)}(\omega_j) = \mathbf{D}_j^H(\mathbf{i}_{K'}^{(l)})\mathbf{h}_{L^{(l)}}^{\mathrm{uc}}(\omega_j) \tag{39}$$

and

$$\mathbf{r}^{(l)}(\omega_j) = \mathbf{r}^{(l-1)}(\omega_j) - \mathbf{b}_{\mathrm{g}}^{(l)}(\omega_j). \tag{40}$$

Finally, we update the masking matrix, $\mathbf{W}^{(l)}$, to be

$$\mathbf{W}^{(l)} = \mathbf{W}^{(l-1)}\mathrm{diag}\left([\mathbf{1}_{L_1}^T\ \mathbf{m}^T\ \mathbf{1}_{L_2}^T]^T\right), \tag{41}$$

where $\mathrm{diag}[\mathbf{x}]$ is a diagonal matrix whose nonzero elements are the entries of the vector $\mathbf{x}$. The vectors $\mathbf{1}_{L_1}$ and $\mathbf{1}_{L_2}$ are vectors of ones of length $L_1(l)$ and $L_2(l)$, respectively, where

$$L_1(l) = m_l^{\mathrm{JSBB}} - \frac{L_{\mathbf{m}}-1}{2} \tag{42}$$

and

$$L_2(l) = M' - m_l^{\mathrm{JSBB}} - \frac{L_{\mathbf{m}}-1}{2}, \tag{43}$$

while $L_{\mathbf{m}}$ is assumed to be odd.

4) Check Compliance to the Constraints: As a stopping criteria, we check whether or not the chosen sensors up to the lth iteration comply the constraints specified in the previous section. To do so, we may solve the following optimization problem, $\forall\omega_j \in \Omega$, separately:

$$\begin{aligned}
&\underset{\mathbf{h}_{L^{(l)}}(\omega_j)}{\text{minimize}} \quad \|\mathbf{h}_{L^{(l)}}(\omega_j)\|_2^2 \\
&\text{subject to} \\
&\quad \mathbf{h}_{L^{(l)}}^H(\omega_j)\,\mathbf{d}_{L^{(l)}}(\omega_j,\theta_{\mathrm{s}}) = 1 \\
&\quad \left\| (b_{\mathrm{d}}^{\mathrm{m}}(\theta_{\mathrm{s}}))^T - \mathbf{h}_{L^{(l)}}^H(\omega_j,)\,\mathbf{D}_{L^{(l)},\Theta_{\mathrm{m}}}(\omega_j) \right\|_2^2 \le \epsilon_1(\omega_j) \\
&\quad \left\| (b_{\mathrm{d}}^{\mathrm{s}}(\theta_{\mathrm{s}}))^T - \mathbf{h}_{L^{(l)}}^H(\omega_j)\,\mathbf{D}_{L^{(l)},\Theta_{\mathrm{s}}}(\omega_j) \right\|_2^2 \le \epsilon_2(\omega_j),
\end{aligned} \tag{44}$$

where $\mathbf{d}_{L^{(l)}}(\omega_j,\theta_{\mathrm{s}}) = \mathbf{T}_{\mathrm{s}}(\mathbf{i}_{K'}^{(l)})\mathbf{d}(\omega_j,\theta_{\mathrm{s}})$, $\mathbf{D}_{L^{(l)},\Theta_{\mathrm{m}}}(\omega_j) = \mathbf{T}_{\mathrm{s}}(\mathbf{i}_{K'}^{(l)})\mathbf{D}_{M,\Theta_{\mathrm{m}}}^H(\omega_j)$, $\mathbf{D}_{L^{(l)},\Theta_{\mathrm{s}}}(\omega_j) = \mathbf{T}_{\mathrm{s}}(\mathbf{i}_{K'}^{(l)})\mathbf{D}_{M,\Theta_{\mathrm{s}}}^H(\omega_j)$, and the vector $\mathbf{h}_{L^{(l)}}(\omega_j)$ is a constrained version of the vector $\mathbf{h}_{L^{(l)}}^{\mathrm{uc}}(\omega_j)$. If we get a valid solution to (44) and also $\|\mathbf{h}_{L^{(l)}}(\omega_j)\|_2^2 \le \gamma(\omega_j)$, $\forall\omega_j \in \Omega$, then we finish, otherwise, we may go back to the second step to choose additional symmetric pair of sensors. As both the objective function and the constraints in (44) are convex, (44) can be solved by convex optimization methods (e.g., using CVX toolbox [54]).

B. Duplicating the Array Layout

The previous step yields the $K' \le K$ indices $\{i_k\}_{k=1}^{K'}$ of sensors that can be used to construct the sparse array layout of a concentric array steered to the endfire direction, i.e., $\theta_{\mathrm{s}} = 0^\circ$. Yet, the main motivation to consider concentric array instead of a more simple geometry like the linear one was due to the rotationally-invariant attribute of concentric arrays. Therefore, we add two more steps to the design. We first duplicate the obtained array layout to $Q-1$ additional directions, meaning that we add a rotated version of the array layout in the following directions: $\frac{2\pi}{Q}, 2\frac{2\pi}{Q}, \ldots, (Q-1)\frac{2\pi}{Q}$. We now have $Z \le QK'$ sensors in the array layout, whose indices are denoted by $\{i_z\}_{z=1}^{Z} \in \mathbf{i}_Z$. This step produces redundancy in both the number of required sensors and the number of required rings. Thus, the next step may apply an optimization in order to obtain a sparse array both in the number of rings, G', and in the total number of sensors, K. Note that, we can use this algorithm also for cases where only a range of angles is desired and not all the azimuthal directions.

C. Optimizing the Number of Rings

As it is assumed that $QK' \ll M$, it is feasible to optimize G' and K for all the relevant bandwidth simultaneously. Moreover, we can save some hardware resources by decimating the number of frequencies by a factor of J_{d}, i.e., the following optimization may be performed over the $J' = J/J_{\mathrm{d}}$ frequencies $\{\omega_j'\}_{j=1}^{J'} = \{\omega_j \mid j \bmod J_{\mathrm{d}} = 0\} \in \Omega$, since the main purpose of this step is to determine the final array layout. Note that a much larger decimation factor may lead to larger deviations in the range between two point. Therefore, in the Simulations section we choose $J_{\mathrm{d}} = 5$, which leads to a smoothed beampattern as illustrated in Fig. 6.

Similarly to the joint-sparse constraint in the greedy part optimization problem (35), a similar constraint should be embedded also to the ℓ_1 optimization problem of that step, ensuring that all the filters $\{\mathbf{h}_K(\omega_j)\}_{j=1}^{J}$ have the same sparse pattern, i.e., the sensors positions which are chosen out of all the candidate positions are common over all the frequencies in the signal's bandwidth of interest Ω. The way to insert such a constraint is by minimizing the ℓ_{12}-norm instead of the ℓ_1-norm [55]. It is defined as the following: suppose we have the vectors $\mathbf{x}_i, i = 1,2,\ldots,n$, of length M, and define $\mathbf{X} = [\mathbf{x}_1, \mathbf{x}_2, \ldots, \mathbf{x}_n]$ to be a matrix containing these vectors in its columns, then the ℓ_{12}-norm of the matrix $\mathbf{X}$ is defined as [56]

$$\|\mathbf{X}\|_{12} \triangleq \sum_{m=1}^{M} \sqrt{\left(\sum_{i=1}^{n} |\mathbf{X}(m,i)|^2\right)}, \tag{45}$$

where $\mathbf{X}(m,i)$ being the entry corresponds to the mth row and the ith column of the matrix $\mathbf{X}$.

Define $\mathbf{h}_Z(\omega_j') = [H_{i_1}(\omega_j'), H_{i_2}(\omega_j'), \ldots, H_{i_Z}(\omega_j')]^T, \omega_j' \in \Omega$ to be vectors of length Z. The entries of each vector are mapped to one of the Z sensors of the original vector $\mathbf{h}(\omega_j)$ (8) whose indices are specified by the vector $\mathbf{i}_Z$. Define $\bar{\mathbf{h}}_g$, $g = 1,\ldots,G$ as vectors containing all the entries of $\mathbf{h}_Z(\omega_j')$ located on the gth ring $\forall\omega_j' \in \Omega$ as

$$\bar{\mathbf{h}}_g = \left\{ \left\{ \{H_{i_z}(\omega_j')\}_{z=1}^{Z} \right\}_{j=1}^{J'} \in\ g\text{th ring} \right\},\ g = 1,2,\ldots,G. \tag{46}$$

Let η_g be an upper limit of the ℓ_2-norm of $\bar{\mathbf{h}}_g$, and employing the concept of the ℓ_{12}-norm introduced by (45), we may define the following iterative optimization problem, which is solved, $\forall\omega_j' \in \Omega$, simultaneously:

$$\begin{aligned}
&\underset{\{\mathbf{h}_Z(\omega_j')\}}{\text{minimize}} \quad \sum_{g=1}^{G} \alpha_g^{(k)} \eta_g \\
&\text{subject to} \quad \eta_g \ge \left\|\bar{\mathbf{h}}_g\right\|_2,
\end{aligned}$$

and $\forall \omega_j' \in \Omega$

$$\begin{aligned}
&\mathbf{h}_Z^H\left(\omega_j'\right)\mathbf{d}_{L_Z}\left(\omega_j',\theta_{\mathrm{s}}'\right)=1\\
&\mathbf{h}_Z^H\left(\omega_j'\right)\mathbf{h}_Z\left(\omega_j'\right)\le\gamma(\omega_j')\\
&\left\|(b_{\mathrm{d}}^{\mathrm{m}}(\theta_{\mathrm{s}}))^T-\mathbf{h}_Z^H\left(\omega_j'\right)\mathbf{D}_{L_Z,\Theta_{\mathrm{m}}'}\left(\omega_j'\right)\right\|_2^2\le\epsilon_1(\omega_j')\\
&\left\|(b_{\mathrm{d}}^{\mathrm{s}}(\theta_{\mathrm{s}}))^T-\mathbf{h}_Z^H\left(\omega_j'\right)\mathbf{D}_{L_Z,\Theta_{\mathrm{s}}'}\left(\omega_j'\right)\right\|_2^2\le\epsilon_2(\omega_j'),
\end{aligned}\tag{47}$$

where $\alpha_m^{(k)}=1/(\eta_m^{(k-1)}+\epsilon)$ for $k>1$ and $\alpha_m^{(1)}=1$, $\eta_m^{(k-1)}$ is the result obtained from the $(k-1)$th iteration, ϵ is a regularization parameter, $\mathbf{d}_{L_Z}(\omega_j',\theta_{\mathrm{s}}')=\mathbf{T}_{\mathrm{s}}(\mathbf{i}_Z)\mathbf{d}(\omega_j',\theta_{\mathrm{s}}')$, $\mathbf{D}_{L_Z,\Theta_{\mathrm{m}}'}(\omega_j')=\mathbf{T}_{\mathrm{s}}(\mathbf{i}_Z)\mathbf{D}_{M,\Theta_{\mathrm{m}}'}(\omega_j')$, and $\mathbf{D}_{L_Z,\Theta_{\mathrm{s}}'}(\omega_j')=\mathbf{T}_{\mathrm{s}}(\mathbf{i}_Z)\mathbf{D}_{M,\Theta_{\mathrm{s}}'}(\omega_j')$. The last equation can be interpreted as a weighted ℓ_1-optimization of the vector $\eta^{(k)}=[\eta_1^{(k)},\eta_2^{(k)},\ldots,\eta_P^{(k)}]^T$, whose gth entry contains the energy of all the selected sensors located on the gth ring, thus, a sparse solution both in the rings and in the sensors is obtained. The optimization is performed for directions $\theta_{\mathrm{s}}'=\theta_{\mathrm{s}}+\frac{\pi}{Q}$, $\Theta_{\mathrm{m}}'=\Theta_{\mathrm{m}}+\frac{\pi}{Q}$, and $\Theta_{\mathrm{s}}'=\Theta_{\mathrm{s}}+\frac{\pi}{Q}$, meaning that the steering direction θ_{s}' is exactly between the direction used by the greedy algorithm of the first step, and the direction of the first duplication of the array layout obtained by the greedy algorithm. Thus, this direction is considered to be the worst case scenario, as it has the largest deviation from the directions used to determine the array layout. Therefore, it ensures that steering to other directions would be also of a high quality.

We run this algorithm iteratively until

$$\Delta\eta\triangleq\frac{\left\|\eta^{(k)}-\eta^{(k-1)}\right\|_2}{\left\|\eta^{(k)}\right\|_2}\le\epsilon_\eta,\tag{48}$$

where ϵ_η is a small positive parameter. Both the vectors $\eta^{(k)}$ and $\{\mathbf{h}_Z(\omega_j')\}_{j=1}^{J'}$ are iteratively updated using (47) until (48) is satisfied. The dominant entries of the vector $\eta^{(k)}$ (i.e., non-zero elements) determine the G' active rings to be used during the synthesis process. The sensors belong to these rings are the K sensors used to construct the desired sparse filters $\{\mathbf{h}_K(\omega_j)\}_{j=1}^J$ satisfying $\mathcal{C}_1,\mathcal{C}_2,\mathcal{C}_3,\mathcal{C}_4,\mathcal{C}_5$, and $\mathcal{C}_6$. The outcome of this iterative algorithm is a joint sparse array layout, both in the number of selected rings, G', and in the total number of selected sensors, K.

D. Synthesis

The goal of the previous steps was to determine the minimal number of the active sensors, K, in a minimal number of rings, G', which fulfill the constraints, using greedy search and ℓ_{12}-norm optimization tools. In the synthesis step, where the K indices $\{i_k\}_{k=1}^K$ of the sensors used to build the FI beampattern were already determined, there is no need to solve an ℓ_1-norm optimization problem and instead we may solve an optimization problem whose objective function is related to constraints $\mathcal{C}_1,\mathcal{C}_2,\mathcal{C}_3,\mathcal{C}_4,\mathcal{C}_5,\mathcal{C}_6$ presented in Section III. A reasonable choice is to minimize the noise output power (i.e., $\mathcal{C}_4$), subject to the constraints, $\mathcal{C}_1,\mathcal{C}_2$, and $\mathcal{C}_3$. Constraints $\mathcal{C}_5$ and $\mathcal{C}_6$ are already embedded in the previous steps. Therefore, we can formulate it as follows: $\forall\omega_j\in\Omega$, solve

$$\underset{\mathbf{h}_K(\omega_j)}{\text{minimize}}\quad\left\|\mathbf{h}_K^H(\omega_j)\right\|_2^2$$

subject to

$$\begin{aligned}
&\mathbf{h}_K^H(\omega_j)\,\mathbf{d}_K(\omega_j,\theta_{\mathrm{s}})=1\\
&\left\|(b_{\mathrm{d}}^{\mathrm{m}}(\theta_{\mathrm{s}}))^T-\mathbf{h}_K^H(\omega_j)\,\mathbf{D}_{K,\Theta_{\mathrm{m}}}(\omega_j)\right\|_2^2\le\epsilon_1(\omega_j)\\
&\left\|(b_{\mathrm{d}}^{\mathrm{s}}(\theta_{\mathrm{s}}))^T-\mathbf{h}_K^H(\omega_j)\,\mathbf{D}_{K,\Theta_{\mathrm{s}}}(\omega_j)\right\|_2^2\le\epsilon_2(\omega_j),
\end{aligned}\tag{49}$$

where $\mathbf{d}_K(\omega_j,\theta_{\mathrm{s}})=\mathbf{T}_{\mathrm{s}}(\mathbf{i}_K)\mathbf{d}(\omega_j,\theta_{\mathrm{s}})$, $\mathbf{D}_{K,\Theta_{\mathrm{m}}}(\omega_j)=\mathbf{T}_{\mathrm{s}}(\mathbf{i}_K)\mathbf{D}_{\Theta_{\mathrm{m}}}(\omega_j)$, and $\mathbf{D}_{K,\Theta_{\mathrm{s}}}(\omega_j)=\mathbf{T}_{\mathrm{s}}(\mathbf{i}_K)\mathbf{D}_{\Theta_{\mathrm{s}}}(\omega_j)$. The resulting filters $\{\mathbf{h}_K(\omega_j)\}_{j=1}^J$ contain the sensors located in the indices $\{\mathbf{p}_{i_k}\}_{k=1}^K$. This fact is important since it means that we can use only K out of M sensors and still obtain adequate results as presented later in Section V.

The proposed design involves the adjustment of several design and tolerance parameters. In [41], we established a procedure for initialization and adjustment of these parameters, which is also relevant to the proposed design. Table I summarizes the user specified parameters. It shows that a much smaller set of parameters should be specified by the user, while most of them are set algorithmically.

TABLE I
USER SPECIFIED PARAMETERS FOR THE PROPOSED ALGORITHM

parameter	initial value
$\{\epsilon_1(\omega_j)\}_{j=1}^J$	Only $\epsilon_1(\omega_1)$ should be determined according to [41]
$\{\epsilon_2(\omega_j)\}_{j=1}^J$	Only $\epsilon_2(\omega_1)$ should be determined according to [41]
$\{\gamma(\omega_j)\}_{j=1}^J$	Only $\gamma(\omega_1)$ should be determined according to [41]
Q	3
J_{d}	5
$\mathbf{m}$	$[0.9\ 0.75\ 0\ 0.75\ 0.9]^T$
ϵ_η	$5\cdot10^{-3}$
ϵ	10^{-4}

Note that the proposed design focuses on the two-dimensional (2D) scenario meaning that it takes into consideration the beampattern in the plane where the array is laid and not across the entire 3D space. Such scenario may lead to simpler solutions with higher performance. Yet, extension of the derivations presented in this work for the 3D scenario is a subject to a future research.

V. NUMERICAL SIMULATIONS

We consider a sparse design of concentric differential microphone arrays (CCDMAs) [6], originally designed with a linear geometry, which combines closely spaced sensors to respond to the spatial derivatives of the acoustic pressure field. These

small-size arrays yield nearly FI beampatterns, and include the well-known superdirective beamformer as a particular case [20]. In spite of their benefits, traditional differential microphone arrays (DMAs) suffer from white noise amplification, especially at low frequencies, and also confined to steering at the endfire direction for linear geometries. For that, we apply a sparse approach for designing robust DMAs with concentric geometries, relatively small numbers of sensors, and nearly rotationally-invariant beampatterns.

As discussed before, we confine ourselves to the case of a 2D beampattern where $\phi = 90^\circ$, i.e., the plane where the array is laid. For that case, the general theoretical expression for the FI beampattern of an Nth-order DMA is given by [44]

$$\mathcal{B}_{\rm d}^{\theta_{\rm s}}(\theta) = \mathcal{B}_N(\theta_{\rm s} - \theta) = \sum_{n=0}^{N} a_{_{N,n}} \cos^n(\theta_{\rm s} - \theta), \qquad (50)$$

where $\{a_{_{N,n}}\}_{n=0}^{N}$ are real coefficients, and the desired signal arrives from the direction $\theta_{\rm s}$. For this example $\mathcal{B}_N(\theta_{\rm s} - \theta)$ is considered to be the desired beampattern. It is assumed that the element spacing, δ, is much smaller than the wavelength of the incoming signal, i.e,

$$\forall \omega \in \Omega: \quad \delta \ll \lambda/2 = \frac{\pi c}{\omega} \Rightarrow \delta \ll \frac{\pi c}{\omega_{\max}}, \qquad (51)$$

in order to approximate the spatial differential of the pressure signal, where $\omega_{\max}$ is the angular frequency corresponding to the highest frequency in the bandwidth of interest, Ω, and $c =$ 340 m/sec.

We assume an initial array geometry consisting of $G = 15$ rings, where the radius of the gth ring is $r_g = (g-1)\delta$, $g = 1, 2, \ldots, G$. We choose uniformly the number of candidate sensors on the gth ring to be

$$M_g = \begin{cases} \frac{\pi}{\arcsin\left(\frac{\sqrt{g-1}\delta}{2r_g}\right)}, & g = 2, \ldots, G \\ 1, & g = 1 \end{cases}, \qquad (52)$$

meaning that the element spacing between two adjacent sensors in the gth ring is $\sqrt{g-1}\delta$. Such a choice of sensor positions leads to a lower density of sensors as the radii of the ring is increased, which is reasonable because sensors from inner rings may contribute to the higher frequencies, while the contribution of sensors from the outer rings is mainly for the lower frequencies, obtaining higher WNG and robustness for the overall FI beampattern. The total number of candidate sensors according to (52) is $M = \sum_{g=1}^{G} M_g = 234$.

We compare between four design approaches. The first one is our proposed greedy sparse design presented in the previous section. The second approach is a uniform one, where K closely uniformly spaced microphones are used to obtain a desired directivity pattern by solving (49). We refer to this approach as the small aperture concentric (SAC) array approach. The third design approach is similar to the second, but with the only difference that the K sensors are spread uniformly over the entire possible concentric aperture of the M candidate sensors. We refer to this approach as the large aperture concentric (LAC) approach. The fourth approach is a random approach, i.e., we choose randomly the K sensors out of M candidate sensors, and solve (49). For that approach, we may average over 100 realizations in order to get a more representative performance level.

We apply the four approaches to designing a FI broadband beampattern for the range of frequencies between $f_{\rm low} =$ 200 Hz and $f_{\rm high} = 8200$ Hz. Assuming a typical duration of $T = 25$ msec for the window analysis used for the corresponding time-domain received signal, the frequency resolution is $\Delta f = 1/T = 40$ Hz. Thus, the number of bins can be calculated as $J = \frac{f_{\rm high} - f_{\rm low}}{\Delta f} = 202$. Note that for such a high number of candidate sensors and frequencies, the proposed greedy sparse design is much more feasible than coherent based sparse design [57], where optimization is performed simultaneously over all frequencies. We choose the element spacing to be $\delta = 1$ cm $\ll \frac{2\pi c}{\omega_{\max}} \approx 4.3$ cm.

We design a third-order hypercardioid pattern (i.e., $N = 3$) which maximizes the directivity factor (DF), whose theoretical beampattern is given according to (50) as [17]

$$\mathcal{B}_N^{\rm HC}(\theta) = -0.14 - 0.57\cos\theta + 0.57\cos^2\theta + 1.15\cos^3\theta, \qquad (53)$$

while we assume that $\theta_{\rm s} = 0^\circ$. In order to build the matrices $\mathbf{D}_{_{M,\Theta_{\rm m}}}(\omega_j)$ and $\mathbf{D}_{_{M,\Theta_{\rm s}}}(\omega_j)$, we uniformly discretize the angular axis with $\Delta\theta = 2^\circ$. For that case we set $\theta_{P'} = 60^\circ$, i.e., the mainlobe region in the azimuthal axis is $-60^\circ \le \theta \le 60^\circ$.

We set initial values for the tolerance parameters $\{\epsilon_1(\omega_j)\}_{j=1}^{J}$, $\{\epsilon_2(\omega_j)\}_{j=1}^{J}$, and $\{\gamma(\omega_j)\}_{j=1}^{J}$, by applying the parameters adjustment procedure introduced in [41]. We also choose the parameters $\epsilon = 10^{-4}$, and $\epsilon_\eta = 5 \cdot 10^{-3}$.

For the proposed incoherent greedy sparse approach, we choose the following mask vector, $\mathbf{m}$, of length $L_{\mathbf{m}} = 5$:

$$\mathbf{m} = [0.9, 0.75, 0, 0.75, 0.9]^T, \qquad (54)$$

which ensures that already selected sensors will not be chosen again, while their neighboring sensors will get lower priority, as this mask is used to update the weighting matrix, $\mathbf{W}^{(l)}$, in its suitable entries according to (41) .

We run the first step of the greedy search in order to find a sparse array layout which yields the desired FI beampattern, while complying the constraints specified in Section III according to the algorithm presented in Section IV-A for the case of steering from the endfire. The array layout obtained by the greedy search, consists of $K' = 26$ sensors, spread over most of the rings, is presented in Fig 2.

The next step is to duplicate the array layout presented in Fig. 2 by a factor of $Q = 3$, meaning that we get a reflected image of the array layout in two more additional directions: $\frac{2\pi}{Q}$ and $\frac{4\pi}{Q}$. Fig. 3 presents the duplicated array layout which is composed of $Z = 72$ sensors.

On that step much more sensors were selected while part of them is unnecessary. Therefore, we apply an ℓ_{12}-norm optimization as presented in Section IV-C, using the CVX software [54]. We set the decimation parameter to be $J_{\rm d} = 5$. After 5 iterations, we get $\Delta\eta < \epsilon_\eta$ and $K = 33$ dominant sensors over $G' = 4$ rings were identified, while all the rest are close to zero, meaning

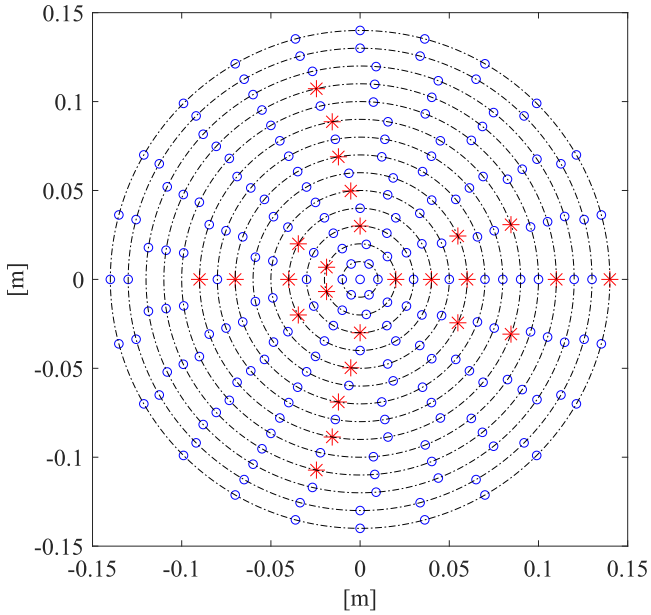

Fig. 2. The array layout obtained by the greedy search. It consists of $K' = 26$ sensors, spread over most of the rings. The blue circles are all the candidate sensors, while the red stars are the selected sensors.

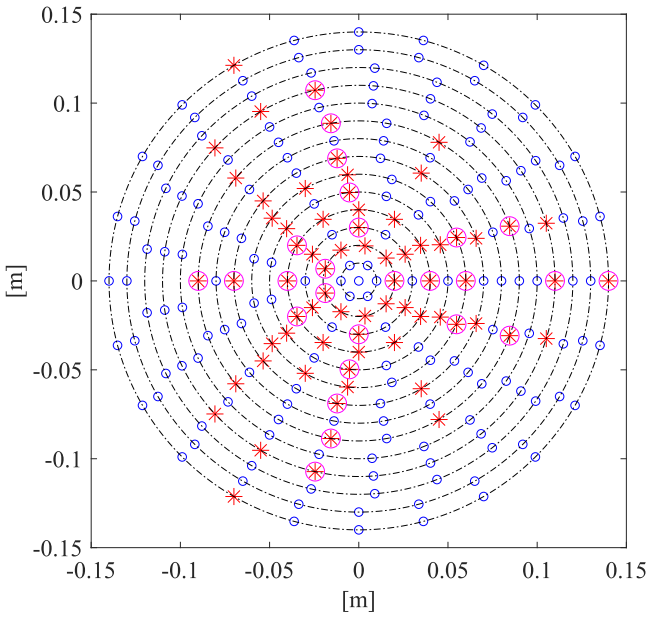

Fig. 3. The array layout after duplication. It consists of $Z = 72$ sensors, spread over most of the rings. The blue circles are all the candidate sensors, the red stars are the selected sensors after duplication, and the pink circles are the sensors obtained by the greedy algorithm of the previous step.

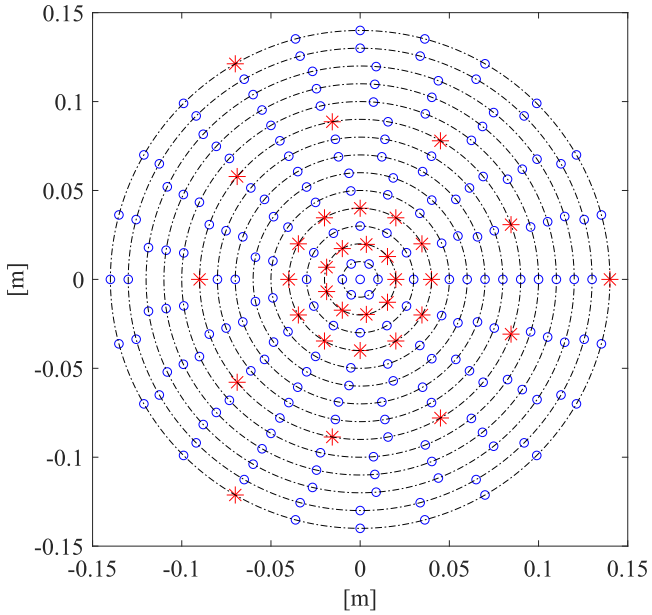

Fig. 4. The array layout of the CCDMAs obtained by the ring optimization procedure presented on Section IV-C. It consists of $K = 33$ sensors, spread over $G' = 4$ rings. The blue circles are all the candidate sensors, while the red stars are the selected sensors.

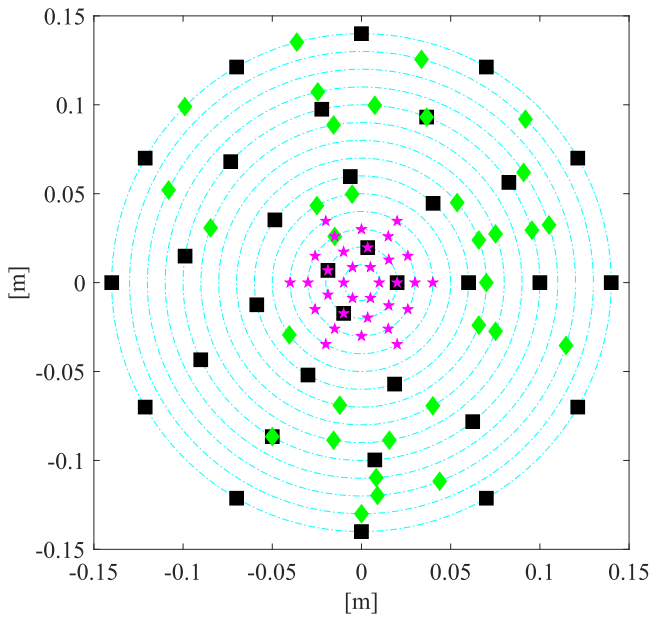

Fig. 5. The array layout of the CCDMAs obtained by uniform and random designs. The black squares are the array layout of the LAC approach, while the pink pentagrams are the array layout obtained by the SAC design. One realization of a random design is presented by the green diamonds.

that both η and the filters $\{\mathbf{h}_Z(\omega'_j)\}_{j=1}^{J'}$ are sparse vectors with $K = 33$ active elements, concentrated in $G' = 4$ rings. The number of selected elements remains the same even if more iterations are used. This iterative optimization problem yields the final array layout presented in Fig. 4. We finally obtain the filters $\{\mathbf{h}_K(\omega_j)\}_{j=1}^{J}$ by solving (49), according to Section IV-D.

Fig. 5 presents the array layout for each of the three remaining approaches. The black squares are the array layout of the LAC approach, while the pink pentagrams are the array layout obtained by the SAC design. One realization of a random design is presented by the green diamonds. For these three approaches, the sensors positions are set a-priori. The SAC approach achieves the smallest array aperture, yet, it suffers from white noise amplification as will be discussed later. Note that comparing the array layout of Fig 4 obtained by the sparse design and the array

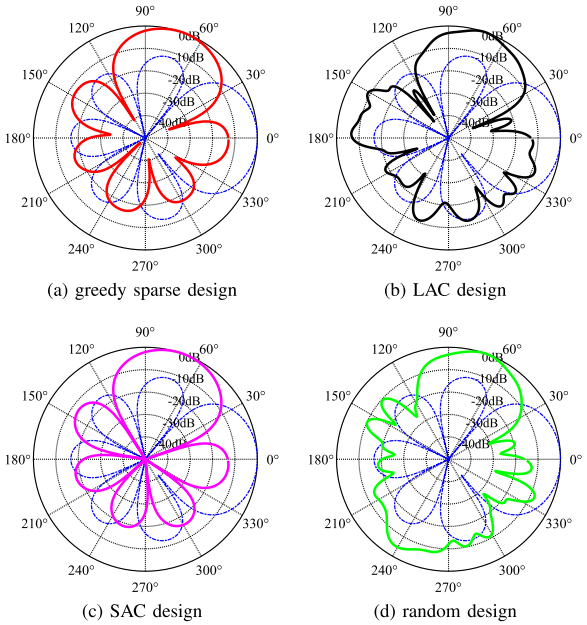

(a) greedy sparse design (b) LAC design

(c) SAC design (d) random design

Fig. 6. Beampatterns of a third-order hypercardioid for $f = 6280$ Hz, steered to $\theta_{\rm s} = 70^\circ$, obtained by the sparse design (red line), the LAC approach (black line), the SAC approach (pink line), and the random design (green line). Also presented is the theoretical beampattern of a third-order hypercardioid (blue dotted line), steered to $\theta_{\rm s} = 0^\circ$.

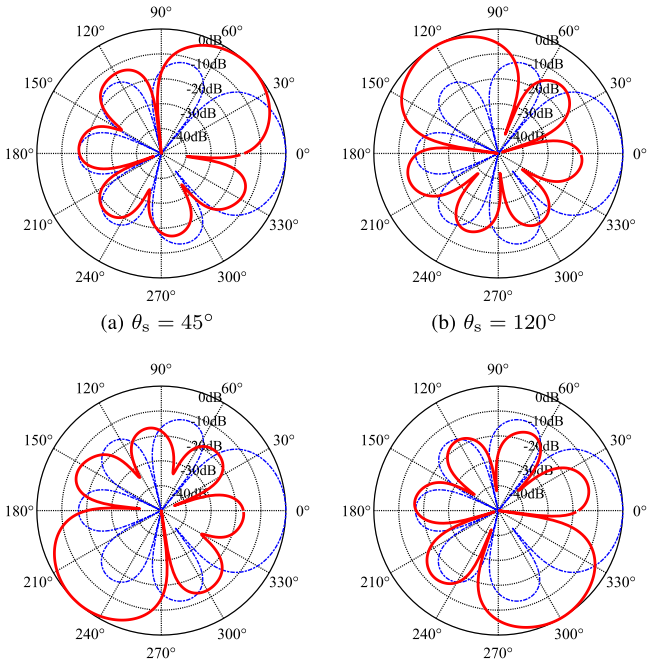

(a) $\theta_{\rm s} = 45^\circ$ (b) $\theta_{\rm s} = 120^\circ$

(c) $\theta_{\rm s} = 225^\circ$ (d) $\theta_{\rm s} = 300^\circ$

Fig. 7. Beampatterns of a third-order hypercardioid obtained by the sparse design (red line) for $f = 4840$ Hz, steered to different values of $\theta_{\rm s}$. Also presented is the theoretical beampattern of a third-order hypercardioid (blue dotted line), steered to $\theta_{\rm s} = 0^\circ$.

layout obtained by other approaches as presented in Fig. 5, one can see that the sparse design offers some kind of compromise between high and low frequencies and panoramic design.

Fig. 6 illustrates the designed beampattern (1) of a third-order hypercardioid for a specific frequency of $f = 6280$ Hz, obtained by each of the four approaches for the case of steering for $\theta_{\rm s} = 70^\circ$. Also presented is the theoretical beampattern (53) of a third-order hypercardioid (blue dotted line) for the case of $\theta_{\rm s} = 0^\circ$. One can see that the SAC approach obtains the beampattern which is the most similar to the theoretical value while the LAC and the random design have much higher sidelobes due to the spatial aliasing. The proposed greedy sparse approach obtains beampattern which is quite similar to the theoretical one.

Fig. 7 shows the beampattern obtained by the proposed sparse design for different steering angles for the case of $f = 4840$ Hz (red solid line). Also presented the theoretical third-order beampattern. One can see that the designed beampattern is rotational-invariant and can be steered to any azimuthal direction.

Fig. 8 shows the WNG (16), the DF (55), and the SLL (57) as a function of frequency obtained by the greedy sparse design (red stars line), the LAC design (black squares line), the SAC design (pink pentagrams line), the random design (green diamonds line), and the theoretical DF of a third-order hypercardioid (blue dashed line). The DF of an array is the gain in signal-to-noise ratio (SNR) for the case of a spherical diffuse noise, i.e. [2]:

$$\begin{aligned}\mathcal{D}\left(\mathbf{h}(\omega_j)\right) &= \frac{\left|\mathcal{B}\left(\mathbf{h}(\omega),\theta_0,\phi_0\right)\right|^2}{\frac{1}{4\pi}\int_0^{2\pi}\int_0^{\pi}\left|\mathcal{B}\left(\mathbf{h}(\omega),\theta,\phi\right)\right|^2\sin\phi d\phi d\theta} \\ &= \frac{\left|\mathbf{h}^H\left(\omega_j\right)\mathbf{d}\left(\omega_j,\theta_{\rm s}\right)\right|^2}{\mathbf{h}^H\left(\omega_j\right)\mathbf{\Gamma}_{\rm dn}\left(\omega_j\right)\mathbf{h}\left(\omega_j\right)},\end{aligned} \tag{55}$$

where $\mathcal{B}(\mathbf{h}(\omega),\theta,\phi)$ is the synthesized 3D directivity pattern,

$$\left[\mathbf{\Gamma}_{\rm dn}\left(\omega_j\right)\right]_{il} = \operatorname{sinc}\left(\frac{\omega_j}{c}d_{i,j}\right) \tag{56}$$

is the $M \times M$ pseudo-coherence matrix of the diffuse noise field, and $d_{i,j}$ is the distance between the ith sensor and the jth sensor. As we focus on the 2D scenario and optimize only the 2D directivity pattern, the presented DF is for the case that the integral in (55) was calculated along the ring of $\phi = \frac{\pi}{2}$, and not across the entire sphere.

We also define the SLL as the integral of the square of the beampattern over the region of the sidelobes, i.e., $\Theta_{\rm s}$, that is,

$$\mathcal{S}\left(\mathbf{h}(\omega_j)\right) = \int_{\theta\in\Theta_{\rm s}}\left|\mathcal{B}\left(\mathbf{h}(\omega_j),\theta,\phi=\frac{\pi}{2}\right)\right|^2 d\theta. \tag{57}$$

One can see that the greedy sparse design obtains superior results in terms of WNG, DF, and SLL with respect to the other approaches. The SAC obtains nearly FI optimal DF implying on its FI beampattern, but achieves poor WNG, especially for low frequencies, which is a well-known problem of superdirective beamformers in general, and of DMAs in particular. The LAC approach obtains higher level of sidelobes in high frequencies, which is reasonable because of the effect of grating lobes which start to appear. Note that the effect of grating lobes in the concentric geometry is much weaker with respect to the case of linear or plannar geometry because in the concentric geometry the sensors in the inner rings are close to each other to prevent or at least to reduce the effect of grating lobes.

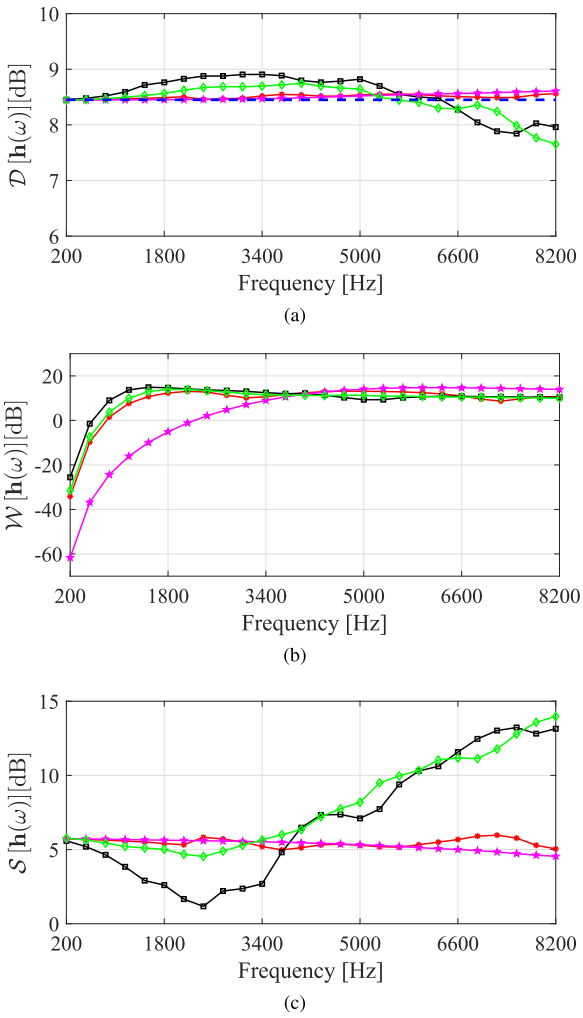

Fig. 8. (a) DF, (b) WNG, and (c) SLL vs. frequency for the greedy sparse design (red circles line), the LAC design (black squares line), the SAC design (pink pentagrams line), and the random design (green diamonds line). Also presented is the theoretical DF of a third-order hypercardioid (blue dashed line).

The WNG presented in Fig. 8 does not suffer from the nulls problem as discussed and presented in [6]. This is obtained by using a concentric structure, which prevents spatial aliasing of the received signal. In order to gain more insight about that we may extend the derivation presented in [6] for the simple case of first-order CCDMAs to the third-order CCDMAs.

Note that although in our design we consider a convex optimization solution (49), analyzing a minimum-norm solution as presented in [6] may still provide some insight as both solutions are related. It was shown there that the minimum-norm solution filter for the case of concentric arrays can be formulated as [6]

$$\mathbf{h}_{\mathrm{MN}}(\omega_j) = \Psi(\omega_j)^H \left[\Psi(\omega_j)\Psi(\omega_j)^H\right]^{-1} \mathbf{b}_{\mathrm{N+1}}, \tag{58}$$

where

$$\Psi(\omega_j) = [\Psi_1(\omega_j)\ \Psi_2(\omega_j)\ \ldots \Psi_G(\omega_j)] \tag{59}$$

is a matrix of size $(N+1)\times\mathcal{M}$, where $\mathcal{M}=\sum_{g=1}^{G}\mathcal{M}_g$, $\mathcal{M}_g = \lfloor M_g/2\rfloor + 1$,

$$\Psi_g(\omega_j) \triangleq \begin{bmatrix} J_0^{'*}(\frac{\omega_j r_g}{c})\boldsymbol{\zeta}_{g,0}^T \\ J_1^{'*}(\frac{\omega_j r_g}{c})\boldsymbol{\zeta}_{g,1}^T \\ \vdots \\ J_N^{'*}(\frac{\omega_j r_g}{c})\boldsymbol{\zeta}_{g,N}^T \end{bmatrix} \tag{60}$$

is an $(N+1)\times\mathcal{M}_g$ matrix, with

$$\boldsymbol{\zeta}_{g,n} \triangleq \left[1\ \cos(n\psi_{g,2})\ldots\cos(n\psi_{g,\mathcal{M}_g})\right]^T$$
$$n=0,1,2,\ldots,N,\ g=1,2,\ldots,G \tag{61}$$

and

$$J_n^{'}(\frac{\omega_j r_g}{c}) = \begin{cases} J_n(\frac{\omega_j r_g}{c}), & n=0 \\ 2j^n J_n(\frac{\omega_j r_g}{c}), & n>0, \end{cases} \tag{62}$$

where $J_n(\cdot)$ is the nth-order Bessel function of the first kind. The vector $\mathbf{b}_{\mathrm{N+1}}$ of length $N+1$ contains the directional constraints.

Similarly to the derivations presented in [6] it can be shown that the correlation matrix $\mathbf{R}(\omega_j)=\Psi(\omega_j)\Psi(\omega_j)^H$ for $N=3$ is given by, Eqn. (63) shown at the bottom of this page.

This matrix contains both diagonal and off-diagonal elements. Substituting the parameters in our simulation, one may observe that the off-diagonal elements are negligible with respect to the diagonal elements. Thus, we can approximate this matrix to be a diagonal matrix whose elements contain summations of Bessel functions, each have zeros in different locations depending on the radii of the rings. Substituting our simulation parameters leading to non overlapping zeros. Thus, this matrix has positive non-zero elements which is invertible and yields a stable solution without nulls.

In Fig. 9 the 3D beampatterns for $f=4040$ Hz are presented for the (a) greedy sparse design, (b) the LAC design, (c) the SAC design, and (d) the random design. One may see the mainbeam on the right side, and the sidelobes on the other size. The trends presented in Fig. 8 can be reflected in the figure. While the sparse design and the SAC approaches have low SLL, both the LAC

$$\mathbf{R}(\omega_j) = \begin{bmatrix} \sum_{g=1}^{G}\mathcal{M}_g\left|J_0^{'}(\frac{\omega_j r_g}{c})\right|^2 & 0 & \sum_{g=1}^{G}J_0^{'*}(\frac{\omega_j r_g}{c})J_2^{'}(\frac{\omega_j r_g}{c}) & 0 \\ 0 & \frac{\sum_{g=1}^{G}(\mathcal{M}_g+1)\left|J_1^{'}(\frac{\omega_j r_g}{c})\right|^2}{2} & 0 & \sum_{g=1}^{G}2J_1^{'*}(\frac{\omega_j r_g}{c})J_3^{'}(\frac{\omega_j r_g}{c}) \\ \sum_{g=1}^{G}J_0^{'*}(\frac{\omega_j r_g}{c})J_2^{'}(\frac{\omega_j r_g}{c}) & 0 & \frac{\sum_{g=1}^{G}(\mathcal{M}_g+2)\left|J_2^{'}(\frac{\omega_j r_g}{c})\right|^2}{2} & 0 \\ 0 & \sum_{g=1}^{G}2J_1^{'*}(\frac{\omega_j r_g}{c})J_3^{'}(\frac{\omega_j r_g}{c}) & 0 & \frac{\sum_{g=1}^{G}(\mathcal{M}_g+2)\left|J_3^{'}(\frac{\omega_j r_g}{c})\right|^2}{2} \end{bmatrix} \tag{63}$$

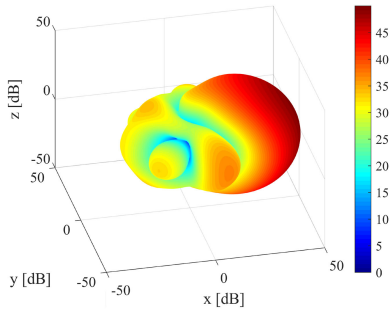

(a) greedy sparse design

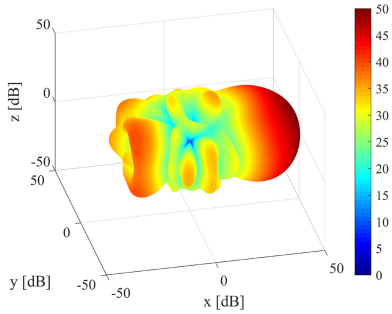

(b) LAC design

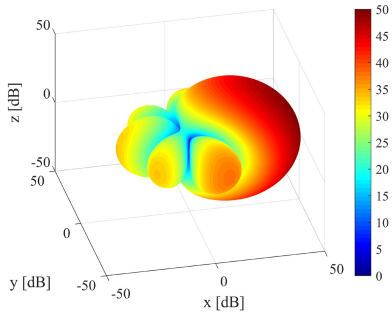

(c) SAC design

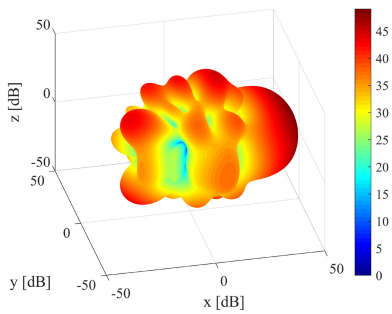

(d) random design

Fig. 9. 3D Beampatterns for $f = 4040$ Hz for the four examined design approaches.

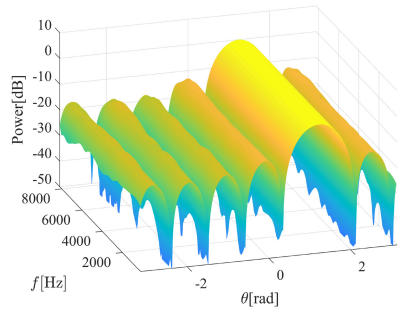

(a) greedy sparse design

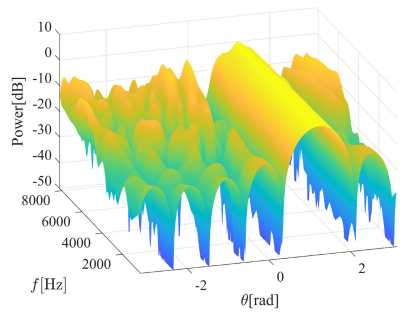

(b) LAC design

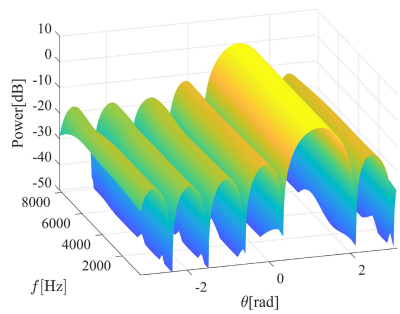

(c) SAC design

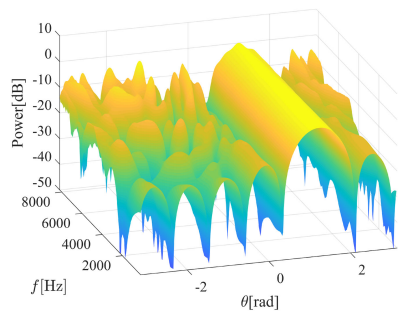

(d) random design

Fig. 10. Beampatterns versus frequency for the four examined design approaches.

and the random approaches suffer from fluctuated and higher SLL.

The synthesized FI beampatterns versus frequency are shown in Fig. 10 for the (a) greedy sparse design, (b) the LAC design, (c) the SAC design, and (d) the random design. This figure reflects the trends inspected by the DF and the SLL plots. Specifically, for the greedy sparse approach the beampattern is almost FI, especially in the mainlobe region and less in the sidelobes regions, as dictated by the constraints $\mathcal{C}_1$ and $\mathcal{C}_2$. The SAC approach achieves the clearest and most perfect FI beampattern, and in the LAC and random designs one can see higher level of sidelobes.

The above design example demonstrates the feasibility and advantages of the greedy sparse approach compared to the uniform and random design approaches.

VI. Conclusion

A greedy sparse design for FI concentric arrays was derived, which supports also the rotationally-invariant property, meaning that almost the same directivity pattern can be designed for different azimuthal directions of steering using the same sparse array layout. The proposed design extends our recent work on incoherent sparse design of FI beamformers where the obtained sparse array layout was not steerable but designed for a fixed steering direction. Moreover, the proposed greedy approach offers more natural and intuitive way to set the number of required sensors in the sparse array layout, which was one of the shortcomings of our previous design. The proposed approach was applied to design a third-order FI robust superdirective DMA with a minimal number of sensors. It was compared to a uniform design and to a random design. Simulations show that the proposed greedy sparse design offers a good compromise between robustness and directivity and obtains rotationally-invariant FI beamformer with a reasonable computational complexity. Future research may focus on different array geometries, extension to the 3D scenario, derivation of joint-sparse versions for multidimensional search algorithms such as genetic algorithms, more advanced greedy algorithms which support the case of coherent dictionaries, and test the proposed design in the presence of some mismatch errors, like gain, phase, and element spacing errors.

Appendix
Calculation of $\mu(\mathbf{D}_j)$ (30)

It can be shown that the mth ($m = 1, \ldots, M$) column of the matrix $\mathbf{D}_j$ has the form of

$$\mathbf{d}_{j_m} = \left[e^{-\jmath \frac{\omega_j r(\mathbf{p}_m)}{c} \cos(\theta_1 - \psi(\mathbf{p}_m))} \ldots \right. \\ \left. e^{-\jmath \frac{\omega_j r(\mathbf{p}_m)}{c} \cos(\theta_P - \psi(\mathbf{p}_m))} \right]^T, \tag{64}$$

where $r(\mathbf{p}_m)$ and $\psi(\mathbf{p}_m)$ denote the radius and angle of the mth sensor located at $\mathbf{p}_m$.

We start by developing the numerator of (27) as

$$\begin{aligned} |\mathbf{d}_{j_l}^H \mathbf{d}_{j_k}| &= \sum_{p=1}^{P} e^{\jmath \frac{\omega_j r(\mathbf{p}_l)}{c} \cos(\theta_p - \psi(\mathbf{p}_l))} e^{-\jmath \frac{\omega_j r(\mathbf{p}_k)}{c} \cos(\theta_p - \psi(\mathbf{p}_k))} \\ &= \sum_{p=1}^{P} e^{\jmath \frac{\omega_j r(\mathbf{p}_l)}{c} [\cos(\theta_p)\cos(\psi(\mathbf{p}_l)) + \sin(\theta_p)\sin(\psi(\mathbf{p}_l))]} \\ &\quad \times e^{-\jmath \frac{\omega_j r(\mathbf{p}_k)}{c} [\cos(\theta_p)\cos(\psi(\mathbf{p}_k)) + \sin(\theta_p)\sin(\psi(\mathbf{p}_k))]} \\ &= \sum_{p=1}^{P} e^{\alpha \cos(\theta_p) + \beta \sin(\theta_p)}, \end{aligned} \tag{65}$$

where

$$\alpha \triangleq \jmath \frac{\omega_j r(\mathbf{p}_l)}{c} \cos(\psi(\mathbf{p}_l)) - \jmath \frac{\omega_j r(\mathbf{p}_k)}{c} \cos(\psi(\mathbf{p}_k)) \tag{66}$$

and

$$\beta \triangleq \jmath \frac{\omega_j r(\mathbf{p}_l)}{c} \sin(\psi(\mathbf{p}_l)) - \jmath \frac{\omega_j r(\mathbf{p}_k)}{c} \sin(\psi(\mathbf{p}_k)). \tag{67}$$

Using the following well-known identity:

$$\int_0^{2\pi} e^{\alpha \cos(\theta) + \beta \sin(\theta)} d\theta = 2\pi I_0(\sqrt{\alpha^2 + \beta^2}), \tag{68}$$

where $I_0(\cdot)$ is the modified Bessel function of the first kind, (65) can be reduced to

$$\sum_{p=1}^{P} e^{\alpha \cos(\theta_p) + \beta \sin(\theta_p)} \approx \frac{2\pi}{\Delta\theta} I_0(\sqrt{\alpha^2 + \beta^2}), \tag{69}$$

where $\Delta\theta$ is the resolution of the azimuthal direction, θ. Therefore,

$$I_0(\sqrt{\alpha^2 + \beta^2}) = I_0\left(\sqrt{-\frac{\omega_j^2}{c^2} \left[r^2(\mathbf{p}_l) + r^2(\mathbf{p}_k) - \mathbf{p}_l^T \mathbf{p}_k \right]} \right), \tag{70}$$

where $\mathbf{p}_l^T \mathbf{p}_k = r(\mathbf{p}_l) r(\mathbf{p}_k) \cos(\psi(\mathbf{p}_l) - \psi(\mathbf{p}_k))$. Finally, we can obtain the following result:

$$\mu(\mathbf{D}_j) = \max_{k \neq l} \left| I_0\left(\sqrt{-\frac{\omega_j^2}{c^2} \left[r^2(\mathbf{p}_l) + r^2(\mathbf{p}_k) - \mathbf{p}_l^T \mathbf{p}_k \right]} \right) \right|. \tag{71}$$

Acknowledgment

The authors thank the associate editor and the anonymous reviewers for their constructive comments and useful suggestions.

References

[1] B. Rafaely, *Fundamentals of Spherical Array Processing*, vol. 8. Berlin, Germany: Springer, 2015.
[2] H. L. Van-trees, *Detection, Estimation and Modulation Theory, Part IV - Optimum Array Processing*. Hoboken, NJ, USA: Wiley, 2002.
[3] J. Benesty, J. Chen, and Y. Huang, *Microphone Array Signal Processing*. Berlin, Germany: Springer-Verlag, 2008.
[4] M. Branstein and D. B. Ward, Eds, *Microphone Arrays: Signal Processing Techniques and Applications*. Berlin, Germany: Springer-Verlag, 2001.
[5] J. Benesty, J. Chen, Y. Huang, and J. Dmochowski, "On microphone-array beamforming from a MIMO acoustic signal processing perspective," *IEEE Trans. Audio, Speech, Lang. Process.*, vol. 15, no. 3, pp. 1053–1065, Mar. 2007.
[6] G. Huang, J. Benesty, and J. Chen, "Design of robust concentric circular differential microphone arrays," *J. Acoustical Soc. America*, vol. 141, no. 5, pp. 3236–3249, 2017.
[7] S. Yan, "Optimal design of FIR beamformer with frequency invariant patterns," *Appl. Acoust.*, vol. 67, pp. 511–528, 2006.
[8] E. Mabande, A. Schad, and W. Kellermann, "Design of robust superdirective beamformer as a convex optimization problem," in *Proc. IEEE Int. Conf. Acoust. Specch Signal Process.*, Taipei, Taiwan, 2009, pp. 77–80.
[9] S. C. Chan and H. H. Chen, "Uniform concentric circular arrays with frequency-invariant characteristics - theory, design, adaptive beamforming and doa estimation," *IEEE Trans. Signal Process.*, vol. 55, no. 1, pp. 165–177, Jan. 2007.

[10] W. Liu and S. Weiss, *Wideband Beamforming: Concepts and Techniques*. Chichester, U.K.: Wiley, 2010.

[11] M. Crocco and A. Trucco, "Design of robust superdirective arrays with a tunable tradeoff between directivity and frequency-invariance," *IEEE Trans. Signal Process.*, vol. 59, no. 5, pp. 2169–2181, May 2011.

[12] B. D. Van Veen and K. V. Buckley, "Beamforming: A versatile approach to spatial filtering," *IEEE Mag. Acoust., Speech, Signal Process.*, vol. 5, pp. 4–24, Apr. 1988.

[13] W. Liu and S. Weiss, "Design of frequency invariant beamformers for broadband arrays," *IEEE Trans. Signal Process.*, vol. 56, no. 2, pp. 855–860, Feb. 2008.

[14] H. Hung and M. Kaveh, "Focusing matrices for coherent signal subspace processing," *IEEE Trans. Acoust. Speech Signal Process.*, vol. 36, no. 8, pp. 1272–1281, Aug. 1988.

[15] Y. Buchris, I. Cohen, and M. A. Doron, "Bayesian focusing for coherent wideband beamforming," *IEEE Trans. Audio, Speech, Lang. Process.*, vol. 20, no. 4, pp. 1282–1295, May 2012.

[16] J. Benesty and J. Chen, *Study and Design of Differential Microphone Arrays*. Berlin, Germany: Springer-Verlag, 2012.

[17] G. W. Elko, "Superdirectional microphone arrays," in *Acoustic Signal Processing for Telecommunication*, S. L. Gay and J. Benesty, Eds. Boston, MA, USA: Kluwer, 2000, ch. 10, pp. 181–237.

[18] M. Buck, "Aspects of first-order differential microphone arrays in the presence of sensor imperfections," *Eur. Trans. Telecommun.*, vol. 13, pp. 115–122, Mar. 2002.

[19] E. De Sena, H. Hacihabiboğlu, and Z. Cavetković, "On the design and implementation of higher order differential microphones," *IEEE Trans. Audio, Speech, Lang. Process.*, vol. 20, no. 1, pp. 162–174, Jan. 2012.

[20] H. Cox, R. M. Zeskind, and T. Kooij, "Practical supergain," *IEEE Trans. Acoust., Speech, Signal Process.*, vol. ASSP-34, no. 3, pp. 393–398, Jun. 1986.

[21] I. J. H. Doles and F. D. Benedict, "Broad-band array design using the asymptotic theory of unequally spaced arrays," *IEEE Trans. Antennas Propagat.*, vol. 36, no. 1, pp. 27–33, Jan. 1988.

[22] D. B. Ward, R. A. Kennedy, and R. C. Williamson, "Theory and design of broadband sensor arrays with frequency invariant farfield beam-patterns," *J. Acoust. Soc. Amer.*, vol. 97, no. 2, pp. 1023–1034, Feb. 1995.

[23] M. Crocco and A. Trucco, "Stochastic and analytic optimization of sparse aperiodic arrays and broadband beamformers with robust superdirective patterns," *IEEE Trans. Audio, Speech, Lang. Process.*, vol. 20, no. 9, pp. 2433–2447, Nov. 2012.

[24] Z. Li, K. F. Cedric Yiu, and Z. Fen, "A hybrid descent method with genetic algorithm for microphone array placement design," *Appl. Soft Comput.*, vol. 13, pp. 1486–1490, 2013.

[25] B. P. Kumar and G. Branner, "Generalized analytical technique for the synthesis of unequally spaced arrays with linear, planar, cylindrical or spherical geometry," *IEEE Trans. Antennas Propag.*, vol. 53, no. 2, pp. 621–634, Feb. 2005.

[26] R. L. Haupt, "Optimized element spacing for low sidelobe concentric ring arrays," *IEEE Trans. Antennas Propag.*, vol. 56, no. 1, pp. 266–268, Jan. 2008.

[27] C. Liu, J. Cai, Z. Huang, X. Wang, and S. Chen, "Pattern synthesis of sparse concentric circular array based on the niche genetic algorithm," in *Proc. IEEE 9th Int. Conf. Commun. Softw. Netw.*, 2017, pp. 906–911.

[28] K. Chen, H. Chen, L. Wang, and H. Wu, "Modified real GA for the synthesis of sparse planar circular arrays," *IEEE Antennas Wireless Propag. Lett.*, vol. 15, no. 1, pp. 274–277,Jun. 2015.

[29] N. N. Pathak, G. K. Mahanti, S. K. Singh, J. K. Mishra, and A. Chakraborty, "Synthesis of thinned planar circular array antennas using modified particle swarm optimization," *Prog. Electromagn. Res.*, vol. 12, pp. 87–97, 2009.

[30] U. Singh and T. Kamal, "Synthesis of thinned planar concentric circular antenna arrays using biogeography-based optimisation," *IET Microw., Antennas Propag.*, vol. 6, no. 7, pp. 822–829, 2012.

[31] A. Chatterjee, G. Mahanti, and P. R. S. Mahapatra, "Optimum ring spacing and interelement distance for sidelobe reduction of a uniform concentric ring array antenna using differential evolution algorithm," in *Proc. IEEE Int. Conf. Commun. Syst.*, 2010, pp. 254–258.

[32] T. N. Kaifas, D. G. Babas, and J. N. Sahalos, "Design of planar arrays with reduced nonuniform excitation subject to constraints on the resulting pattern and the directivity," *IEEE Trans. Antennas Propag.*, vol. 57, no. 8, pp. 2270–2278, Aug. 2009.

[33] X. Zhao, Q. Yang, and Y. Zhang, "A hybrid method for the optimal synthesis of 3-d patterns of sparse concentric ring arrays," *IEEE Trans. Antennas Propag.*, vol. 64, no. 2, pp. 515–524, Feb. 2015.

[34] A. F. Morabito and P. G. Nicolaci, "Optimal synthesis of shaped beams through concentric ring isophoric sparse arrays," *IEEE Antennas Wireless Propag. Lett.*, vol. 16, no. 1, pp. 979–982, Oct. 2016.

[35] L. Zhang, Y.-C. Jiao, and B. Chen, "Optimization of concentric ring array geometry for 3d beam scanning," *Int. J. Antennas Propag.*, vol. 2012, 2012, Art. no. 625437.

[36] P. Angeletti, G. Toso, and G. Ruggerini, "Array antennas with jointly optimized elements positions and dimensions Part ii: Planar circular arrays," *IEEE Trans. Antennas Propag.*, vol. 62, no. 4, pp. 1627–1639, Apr. 2013.

[37] L. Zhang, Y.-C. Jiao, B. Chen, and Z.-B. Weng, "Design of wideband concentric-ring arrays with three-dimensional beam scanning based on the optimization of array geometry," *Electromagn.*, vol. 32, no. 6, pp. 305–320, 2012.

[38] R.-Q. Wang and Y.-C. Jiao, "Synthesis of wideband rotationally symmetric sparse circular arrays with multiple constraints," *IEEE Antennas Wireless Propag. Lett.*, vol. 18, no. 5, pp. 821–825, May 2019.

[39] M. D. Gregory, F. A. Namin, and D. H. Werner, "Exploiting rotational symmetry for the design of ultra-wideband planar phased array layouts," *IEEE Trans. Antennas Propag.*, vol. 61, no. 1, pp. 176–184, Jan. 2012.

[40] Y. Li, K. Ho, and C. Kwan, "3-d array pattern synthesis with frequency invariant property for concentric ring array," *IEEE Trans. Signal Process.*, vol. 54, no. 2, pp. 780–784, Feb. 2006.

[41] Y. Buchris, A. Amar, J. Benesty, and I. Cohen, "Incoherent synthesis of sparse arrays for frequency-invariant beamforming," *IEEE/ACM Trans. Audio, Speech, Lang. Process.*, vol. 27, no. 3, pp. 482–495, Mar. 2019.

[42] Y. C. Pati, R. Rezaiifar, and P. S. Krishnaprasad, "Orthogonal matching pursuit: Recursive function approximation with applications to wavelet decomposition," in *Proc. 27th Asilomar Conf. Signals, Syst. Comput*, 1993, pp. 40–44.

[43] S. G. Mallat and Z. Zhang, "Matching pursuits with time-frequency dictionaries," *IEEE Trans. Signal Process.*, vol. 41, no. 12, pp. 3397–3415, Dec. 1993.

[44] J. Benesty, J. Chen, and I. Cohen, *Design of Circular Differential Microphone Arrays*. Berlin, Germany: Springer-Verlag, 2015.

[45] J. A. Tropp, A. C. Gilbert, and M. J. Strauss, "Algorithms for simultaneous sparse approximation. Part i: Greedy pursuit," *Signal Process.*, vol. 86, no. 3, pp. 572–588, 2006.

[46] J. D. Blanchard, M. Cermak, D. Hanle, and Y. Jing, "Greedy algorithms for joint sparse recovery," *IEEE Trans. Signal Process.*, vol. 62, no. 7, pp. 1694–1704, 2014.

[47] S. Sarvotham, D. Baron, M. Wakin, M. F. Duarte, and R. G. Baraniuk, "Distributed compressed sensing of jointly sparse signals," in *Proc. Asilomar Conf. Signals, Syst., Comput.*, 2005, pp. 1537–1541.

[48] E. J. Candè;s, M. B. Wakin, and S. P. Bond, "Enhancing sparsity by reweighted ℓ_1 minimization," *J. Fourier Analy. Appl.*, vol. 14, pp. 877–905, Dec. 2008.

[49] J. A. Tropp, "Just relax: Convex programming methods for identifying sparse signals in noise," *IEEE Trans. Inf. Theory*, vol. 52, no. 3, pp. 1030–1051, 2006.

[50] J. A. Tropp, "Greed is good: Algorithmic results for sparse approximation," *IEEE Trans. Inf. Theory*, vol. 50, no. 10, pp. 2231–2242, 2004.

[51] R. Giryes and M. Elad, "Omp with highly coherent dictionaries," in *Proc. 10th Int. Conf. Sampling Theory Appl.*, 2013, pp. 9–12.

[52] E. J. Candes, Y. C. Eldar, D. Needell, and P. Randall, "Compressed sensing with coherent and redundant dictionaries," *Appl. Comput. Harmon. Anal.*, vol. 31, no. 1, pp. 59–73, 2011.

[53] R. Heckel and H. Bölcskei, "Joint sparsity with different measurement matrices," in *Proc. 50th Annu. Allerton Conf. Commun., Control, Comput.*, 2012, pp. 698–702.

[54] M. Grant, S. Boyd, and Y. Ye, "CVX: Matlab software for disciplined convex programming," ver. 2.2, Jan. 2008. [Online]. Available: http://cvxr.com/cvx/download/

[55] P. T. Boufounosa, P. Smaragdisb, and B. Rajc, "Joint sparsity models for wideband array processing," in *Proc. SPIE Opt. Eng.+ Appl.*, 2011, pp. 81 380–K.

[56] S. F. Cotter, B. D. Rao, K. Engan, and K. Kreutz-Delgado, "Sparse solutions to linear inverse problems with multiple measurement vectors," *IEEE Trans. Signal Process.*, vol. 53, no. 7, pp. 2477–2488, Jul. 2005.

[57] Y. Liu, L. Zhang, L. Ye, Z. Nie, and Q. H. Liu, "Synthesis of sparse arrays with frequency-invariant-focused beam patterns under accurate sidelobe control by iterative second-order cone programming," *IEEE Trans. Antennas Propagat.*, vol. 63, no. 12, pp. 5826–5832, Dec. 2015.

Yaakov Buchris (Member, IEEE) received the B.Sc. and M.Sc. degrees in electrical engineering from the Technion Israel Institute of Technology, Haifa, Israel, in 2005 and 2011, respectively. He is currently working toward the Ph.D. degree in electrical engineering with the Technion-Israel Institute of Technology, Haifa, Israel.

Since 2002, he has been with RAFAEL, Advanced Defense Systems Ltd, Haifa, Israel, as a Research Engineer in the underwater acoustic communication group. Since 2005, he has also been a Teaching Assistant and a Project Supervisor with the Communications Lab and the Signal and Image Processing Lab (SIPL), Electrical Engineering Department, Technion. His research interests are statistical signal processing, adaptive filtering, digital communications, and array processing.

Israel Cohen (Fellow, IEEE) received the B.Sc. (*Summa Cum Laude*), M.Sc., and Ph.D. degrees in electrical engineering from the Technion—Israel Institute of Technology, Haifa, Israel, in 1990, 1993 and 1998, respectively. He is a Professor of electrical engineering with the Technion—Israel Institute of Technology, Haifa, Israel.

From 1990 to 1998, he was a Research Scientist with RAFAEL Research Laboratories, Haifa, Israel Ministry of Defense. From 1998 to 2001, he was a Postdoctoral Research Associate with the Computer Science Department, Yale University, New Haven, CT, USA. In 2001, he joined the Electrical Engineering Department of the Technion. He is a Co-Editor of the Multichannel Speech Processing Section of the *Springer Handbook of Speech Processing* (Springer, 2008), and a Co-Author of *Fundamentals of Signal Enhancement and Array Signal Processing* (Wiley-IEEE Press, 2017). His research interests are array processing, statistical signal processing, analysis and modeling of acoustic signals, speech enhancement, noise estimation, microphone arrays, source localization, blind source separation, system identification and adaptive filtering.

Dr. Cohen was awarded the Norman Seiden Prize for Academic Excellence (2017), the SPS Signal Processing Letters Best Paper Award (2014), the Alexander Goldberg Prize for Excellence in Research (2010), and the Muriel and David Jacknow Award for Excellence in Teaching (2009). He is currently an Associate Member of the IEEE Audio and Acoustic Signal Processing Technical Committee. He was an Associate Editor for the IEEE TRANSACTIONS ON AUDIO, SPEECH, AND LANGUAGE PROCESSING and IEEE SIGNAL PROCESSING LETTERS, and a member of the IEEE Audio and Acoustic Signal Processing Technical Committee and the IEEE Speech and Language Processing Technical Committee.

Jacob Benesty received the master's degree in microwaves from Pierre & Marie Curie University, Paris, France, in 1987, and the Ph.D. degree in control and signal processing from Orsay University, Orsay, France, in April 1991. During the Ph.D. (from November 1989 to April 1991), he worked on adaptive filters and fast algorithms with the Centre National d'Etudes des Telecomunications, Paris, France. From January 1994 to July 1995, he worked with Telecom Paris University on multichannel adaptive filters and acoustic echo cancellation. From October 1995 to May 2003, he was first a Consultant and then a Member of the Technical Staff at Bell Laboratories, Murray Hill, NJ, USA. In May 2003, he joined the University of Quebec, INRS-EMT, in Montreal, Quebec, Canada, as a Professor. He is an Adjunct Professor with Aalborg University, Denmark, and a Guest Professor with Northwestern Polytechnical University, Xi'an, China.

He has co-authored and co-edited/co-authored numerous books in the area of acoustic signal processing. His research interests are in signal processing, acoustic signal processing, and multimedia communications. He is the Inventor of many important technologies. In particular, he was the Lead Researcher with Bell Labs who conceived and designed the world-first real-time hands-free full-duplex stereophonic teleconferencing system. Also, he conceived and designed the world-first PC-based multi-party hands-free full-duplex stereo conferencing system over IP networks.

Dr. Benesty is an Editor of the book series *Springer Topics in Signal Processing*. He was the General Chair and the Technical Chair of many international conferences and a member of several IEEE technical committees. Four of his journal papers were awarded by the IEEE Signal processing Society and in 2010 he received the Gheorghe Cartianu Award from the Romanian Academy.

Alon Amar (Member, IEEE) received the B.Sc. degree in electrical engineering from the Technion-Israel Institute of Technology, Haifa, Israel, in 1997 and the M.Sc. degrees in electrical engineering from Tel Aviv University, Tel Aviv, Israel, in 2003, and 2009, respectively. From 2009 to 2010, he was a Postdoctoral Research Associate with the Circuits and Systems group, Faculty of Electrical Engineering, Mathematics, and Computer Science, Delft University of Technology, Delft, The Netherlands. In 2011, he joined the Israeli National Research Center, Haifa, as a Research Scientist. Since 2016, he is an Adjunct Lecturer and a Research Associate with the Department of Electrical Engineering, Technion, Israel Institute of Technology, Haifa, Israel. His main research interests include statistical and array signal processing, wireless communication, and sensor networks.